Supplementary Materials for

Counteracting age-related VEGF signaling insufficiency promotes healthy aging and extends life span

M. Grunewald*, S. Kumar†, H. Sharife†, E. Volinsky†, A. Gileles-Hillel, T. Licht,
A. Permyakova, L. Hinden, S. Azar, Y. Friedmann, P. Kupetz, R. Tzuberi, A. Anisimov,
K. Alitalo, M. Horwitz, S. Leebhoff, O. Z. Khoma, R. Hlushchuk, V. Djonov, R. Abramovitch,
J. Tam, E. Keshet*

*Corresponding author. Email: myriamg@ekmd.huji.ac.il (M.G.);
elik@ekmd.huji.ac.il (E.K.)
†These authors contributed equally to this work.

This PDF file includes:

Materials and Methods
Figs. S1 to S19
Tables S1 to S4
Captions for Data S1 to S19
References

Other Supplementary Material for this manuscript includes the following:
(available at science.sciencemag.org/content/373/6554/eabc8479/suppl/DC1)

Data S1 to S9 (Excel)
MDAR Reproducibility Checklist (PDF)

Materials and Methods

Mice strains

Transgenic VEGF and control mice originated from transgenic BALB/cOlaHsd mice, which were backcrossed into C57BL/6J background for more than 10 generations. Transgenic mice were maintained as heterozygous and colonies were refreshed by backcrossing to C57BL/6JRccHsd new breeders (see (*35*) for details on this specific strain obtained from Envigo RMS Israel). The genetic background of parents and littermates used in this study was retrospectively verified by single nucleotide polymorphism (SNP) analysis (performed at the Jackson laboratory) and was found to contain 0.7 to 1.4 % Balb/cJ into C57BL6 background (19.26 to 25% C57BL6/NJ and 75 to 80.74% C57BL6/J).

Transgenic VEGF production by hepatocytes was induced in a bi-transgenic 'Tet-off' system composed of a 'driver' line in which a tetracycline-regulated transactivator (tTA) protein is driven by a C/EBPβ (also known as liver-activator protein (LAP) promoter (*36*) and a 'responder' tetracycline-responsive promoter element (TRE) -VEGF-A164 line (*37*). To keep the system in the 'off' mode 500µg/ml tetracycline (tetracycline hydrochloride TB0504, Biobasic) is usually added to the drinking water in breeding cages and from weaning onwards and transgenic VEGF is induced by removal of tetracycline. We found that during adulthood, the system is somewhat leaky and low levels of VEGF are also released to the circulation in the intended 'off' mode in some litters. With the aim of reproducibly attain a low level of circulating transgenic VEGF, we used a limited level of tetracycline (320 µg/ml), from weaning onwards. Levels of circulating VEGF were measured bimonthly using a mouse specific VEGF ELISA (R&D) and were found to be in the range of 80-250 pg/ml. Littermates resulting from a [heterozygous driver: heterozygous responder] mating who have inherited only one of the transgenes, and grown in the same cage, served as controls. To obtain sufficiently large number of double-transgenic VEGF mice, each male mouse was housed together with 2-3 female mice and offspring's born in the same day were considered as a single litter. The genetic composition of each individual mouse used for survival studies, arranged by litter, is indicated in tables S1 and S2.

Transgenic sFlt1 and control mice are on a BALB/cOlaHsd background. A soluble form of the human VEGFR1 (sFlt1) consisting of the extracellular part of the receptor, acting as a decoy receptor for VEGF, was conditionally induced in endothelial cells using a bi-transgenic 'Tet-off' system with Cdh5 promoter-tTA (*38*) serving as the driving transgene and a TRE-sFlt1 as the responder transgene (*14,30*). Double-transgenic mice were kept in the 'off' mode by inclusion of 500 µg/ml Tetracycline (TB0504, Biobasic in 3% sucrose) in the drinking water and sFlt1 was induced at the indicated ages by Tetracycline withdrawal. Levels of hsFlt1 induced were determined periodically using a human specific VEGFR1 ELISA (R&D).

Adeno-Associated Virus (AAV)- mediated VEGF delivery: Recombinant Adeno-Associated Viral vectors (AAV, serotype 9) encoding mouse VEGF164 (AAV-VEGF) or scrambled control sequence (AAV-Control) were constructed and amplified as described previously (*39*) but using the Open Reading Frame of VEGF-A 164 (Genbank sequence NM_009505). Low titers of virus were injected intraperitoneally at a titer of 5.107 vp in150 µl sterile saline onto C57BL/6JRccHsd (Envigo RMS Israel). Infection efficiency was verified by measuring VEGF circulating levels using VEGF ELISA (R&), from two

weeks following the injection and monthly thereafter. Infection efficiency was verified by measuring VEGF circulating levels using ELISA, two weeks following the injection and monthly thereafter.

General mouse procedures

All animal procedures were performed in accordance with the Hebrew University of Jerusalem Institutional Animal Care and Use Committee guidelines under animal ethics protocols MD-15513-5.

Mice were housed in a SPF facility with controlled temperature and humidity on 12 h light/dark cycles and fed Ad-libitum with regular rodent's chow.

The number of animals shown in each figure is indicated as n = x mice/group.

Mice used for lifespan measurements were maintained until near end of life and were euthanized when clinical signs suggested death within 24 hours (except for censored mice). A complete necropsy was performed on all mice and discernable tumors were recorded.

For complete blood counts, blood was drawn from the tail vein and at the time of sacrifice, by cardiac puncture. Blood was collected into EDTA-coated collection tubes (BD, K2E microtainers) and analyzed by a Mindray BC-2800 Vet hematology analyzer. Plasma was separated by centrifugation for 20 mn at 2000g.

ELISA

The following commercially available ELISA kits were used to measure protein levels in plasma and tissue lysates: mouse VEGF- Quantikine ELISA kit (R&D Systems; MV00), mouse VEGF Receptor 1- Quantikine ELISA kit (R&D Systems; MVR100), human VEGF Receptor 1 -Quantikine ELISA kit (R&D Systems; DVR100B), mouse C- reactive Protein - Quantikine Elisa kit (R&D Systems MCRP00) and mouse MCP1- Quantikine Elisa kit (R&D systems MJE00B). Tissue lysates for ELISA were homogenized in PBS using a Next Advance Bullet Blender homogenizer, stored overnight at −20°C, and lysed by two freeze–thaw cycles followed by centrifugation for 5 min at 5,000 g and supernatant collection. Bradford assay was used to standardize tissue lysate concentrations according to the manufacturer's instructions (Bio-Rad Protein Assay Dye Reagent Concentrate; 500-0006). ELISAs were read at 450 nm with a reference value of 540 nm using a Tecan Infinite f200 Pro 96-well plate reader.

Liver enzymes level measurement in serum

Serum alanine aminotransferase (ALT) and aspartate aminotransferase (AST) levels were determined using COBAS C-111 chemistry analyzer (Roche, Switzerland)

Immunoprecipitation and Western Blot

Indicated organs, harvested at the specified ages, were homogenized in lysis buffer (20mM Tris HCl [pH 8], 137 mM NaCl, 1% Nonidet P-40 and 2mM EDTA) supplemented with protease inhibitor cocktail (SIGMAFAST, Merck) and phosphatase inhibitor cocktail (PhosSTOP, Merck). For immunoprecipitation, 1 mg of total protein was diluted to a volume of 1 ml and incubated overnight at 4 °C with 10 µl VEGFR2 antibody (Cell Signaling #2479) bound to 100 µl of Protein A-agarose beads (Santa Cruz Biotechnology, #sc-2001). The next day, beads were washed 3 times in lysis buffer and

were further boiled in 100 µl of 1X SDS buffer (50 mM Tris HCl [pH 6.8], 2% SDS, 6% Glycerol, 0.004 % Bromophenol blue and 1% β-Mercaptoethanol). Immunoprecipitates were resolved by 4-20% SDS-PAGE gel (Bio-rad, #4568094) and transferred onto nitrocellulose membrane using Trans-Blot Turbo transfer system (Bio-rad, #1704159). The membranes were then incubated in blocking buffer (3% BSA in 1X Tris buffered saline with 0.1% Tween 20 [TBST]) for 2 h at room temperature followed by overnight incubation with the following antibodies: p-VEGFR2 (Cell Signaling #2478, 1:500) or VEGFR2 (Cell Signaling #2479, 1:500) at 4 ᵒC. The following day, the membranes were washed 3X with washing buffer (1X TBST) and incubated with appropriate HRP-conjugated secondary antibody (Cell Signaling #7074, 1:1000) for 2 h at room temperature. Signal was detected using chemiluminescent HRP substrates (Supersignal West Pico/Femto, Thermo Fisher Scientific, Millipore). Imaging and quantification of signal was done using ChemiDocTMXRS+ imager.

RNA isolation and cDNA preparation
Tissues were homogenized using a Next Advance Bullet Blender homogenizer and RNA was isolated using TriReagant (Sigma) according to the manufacturer's instructions. RNA was quantified using a Nanodrop spectrophotometer.
cDNA was prepared using a high-capacity cDNA reverse transcription kit (iScript cDNA synthesis kit (Biorad) with RNase inhibitor according to the manufacturer's instructions.

Quantitative PCR
FAST SYBR Green Master Mix (Applied Biosystems) was used for qPCR according to the manufacturer's instructions. Real-time PCR was performed on an Applied Biosystems StepOne Plus qPCR machine. An extra dissociation step was added. qPCR results were analyzed using StepOne Plus Software v2.3 (Applied Biosystems).
Expression of all genes was normalized to GAPDH except for mP16 that was normalized to HPRT.
Primers were designed by using Nucleotide database (NCBI). Primers were synthesized by Integrated DNA Technologies. The sequences for the primers used were as follows:
m-Flt-F: GGGTGTCTATAGGTGCCGAG
m-Flt-R: AGCCAAAAGAGGGTCGCA
m-sFlt1-F: TCTAGAAGACTCGGGCACCTATG
m-sFlt1-R: CGCAGTGCTCACCTCTAACG
mCDH5-F: TCCTCTGCATCCTCACTATCA
mCDH5-R: GTAAGTGACCAACTGCTCGTG
mGAPDH-F: CCTGGAGAAACCTGCCAAG
mGAPDH-R: CAACCTGGTCCTCAGTGTAGC
mP16INK4a expression analysis was performed using Taqman Master Mix (Applied Biosystems) according to manufacturer's instructions, using the following primers
mP16-F:CGGTCGTACCCCGATTCAG
mP16-R: GCACCGTAGTTGAGCAGAAGAG.
Relative gene expression was normalized to HPRT with commercially provided primers (Thermo Fisher- 4331182).

Tissue section staining

5-µm paraffin sections were cut from indicated organs at specified ages as indicated in the figure legends. Paraffin-embedded tissue sections were stained with hematoxylin and eosin (H&E) for routine examination.

For analysis of skin sections, 5-µm paraffin sections from dorsal skin flaps were stained with Masson-Trichome (Diagnostic Biosystems #KT034) highlighting muscle and intercellular fibers in red, nuclei in black and collagen in blue.

For Oil-red-O staining, non-fixed tissue was embedded in OCT (Tissue-Tek) and frozen in liquid nitrogen. 10µm-thick slices were prepared using a Leica CM1950 cryostat and stored at -80°C until used. Sections were then immersed in Oil Red O working solution (0.5% Oil red O (Sigma o0625) in isopropanol) for 30min and counterstained with Hematoxylin. The relative area covered by red-stained oil droplets was calculated using an ImageJ software.

For SA-β-gal activity cryosection staining, freshly prepared liver cryosections (Leica CM1950 cryostat) were fixed with 0.5% glutaraldehyde in PBS for 15 min, washed with PBS supplemented with 1 mM $MgCl_2$, and stained for 6–8 h in X-Gal staining solution ($PBS/MgCl_2$, 0.2M $K_3Fe(CN)_6$, 0.2M $K_4Fe(CN)_6$ $3H_2O$, X-Gal) and counterstained with Nuclear Fast Red (Sigma).

For immunostaining, antigen retrieval was performed by citrate buffer (pH 6; Zymed Laboratories) in a pressure cooker. Sections were then blocked in 1% BSA and 0.5% Triton X-100. Primary antibodies used were: anti-mouse sFlt1 (INVITROGEN #36-1100), anti-mouse CD31 (ABCAM #ab28364), anti-mouse UCP1 (ABCAM #ab10983). Sections were incubated overnight in primary antibody diluted in 1% BSA and 0.5% Triton X-100 at 4°C. Universal anti mouse and rabbit Ig was used as a secondary antibody according to the manufacturer's instruction (ImmPress Reagent Kit peroxidase #MP7500- Vector). Peroxidase activity was detected using AEC staining kit according to the manufacturer (Sigma #AEC101-1KT). Sections were counterstained by standard Hematoxylin (Meyer's hematoxilin (Sigma)).

Fluorescent lectin (Vector # DL-1207) was used to detect capillaries in brown adipose tissues. Sections were mounted with Permafluor mounting medium containing DAPI (Thermo Fisher Scientific). Confocal images were taken using an Olympus FV-1000 Confocal and images were analyzed with FV10-ASW 3.0 Viewer and ImageJ software.

Microvascular density (MVD) and perfusion mapping

MVD was calculated from CD31- or lectin- stained tissue sections using ImageJ software and expressed as the relative area covered by stained capillaries. Each dot in the graphs represents the average of measures obtained from 7 to 10 fields in 2 different tissue sections per mouse.

For perfusion mapping, perfused vessels were selectively labelled by tail vein injection of a solution containing 0.16 µg of Alexa-Fluor 647 conjugated CD144 antibody (Biolegend, BV13) per gram of body weight, 10 minutes before mice were euthanized by overdose of anesthetics Ketanest (100mg/kg) and Rompun (10mg/kg). Mice were perfused through the left ventricle with 20 ml of PBS and then with 60 ml of ice-cold fixing solution (4% buffered Paraformaldehyde, pH-7.36). Fixed tissues were harvested and left in 30% sucrose in 4% PFA solution for 24 hours at 4°C. Tissues were

then embedded in OCT, snap frozen in liquid nitrogen and cryosectioned. 50μm-thick Z-stacked images were captured using a Zeiss LSM 710 confocal microscope and the relative area covered by stained capillaries was calculated using Image Pro-Plus analysis software (Media Cybernetics).

Ultrasound and Photoacoustic imaging
High-resolution ultrasound imaging was performed using a Vevo3100- LAZRX small animal US combined with photoacoustic (PA) imaging system (Visualsonics, Toronto, Canada), with a MX-550D linear-array transducer (40-MHz center frequency) used to acquire all images. A tunable laser supplied 10–20 mJ per pulse over the 680– 970-nm wavelength range, with a pulse repetition frequency of 20 Hz. Once initialized, the system was switched to the oxy/hemo mode to measure sO_2 using the following parameters: depth, 10.00 mm; width, 14.08 mm; wavelength, 750 and 850 nm for the total hemoglobin concentration threshold (Hbt), and sO_2, respectively. For presentation, hind limb sO_2 maps were pseudo-colored. Mice analyzed were anesthetized with isoflurane (2.0%) and placed in a supine position on a heated platform, with body temperature, heart rate, and respiration rate monitored. All images were acquired by placing the probe directly over the right hind limb. Before sO_2 measurement, B-mode and Doppler US images were acquired to evaluate femoral artery blood flow and identify the region of interest in the hind limb muscle. The peak systolic velocity (Vs) and the minimal end diastolic velocity (Vd) were calculated over an average of three cardiac cycles using Vevo Lab software.

Body composition analysis
Total body fat and lean masses were determined by EchoMRI-100H™ (Echo Medical Systems LLC, Houston, TX, USA).

Multi-parameter metabolic assessment
Metabolic and activity profiles of the mice were assessed by using the Promethion High-Definition Behavioral Phenotyping System (Sable Instruments, Inc., Las Vegas, NV, USA) as described previously (40). Briefly, mice with free access to food and water were subjected to a standard 12 h light/12 h dark cycle, which consisted of a 48 h acclimation period followed by 24 h of sampling. Respiratory gases were measured by using the GA-3 gas analyzer (Sable Systems, Inc., Las Vegas, NV, USA) using a pull- mode, negative-pressure system. Air flow was measured and controlled by FR-8 (Sable Systems, Inc., Las Vegas, NV, USA), with a set flow rate of 2000 mL/min. Water vapor was continuously measured and its dilution effect on O2 and CO2 was mathematically compensated. Effective body mass was calculated by ANCOVA analysis. Respiratory quotient (RQ) was calculated as the ratio of VCO2/VO2, and total energy expenditure (TEE) was calculated as VO2 x (3.815 + 1.232 x RQ), normalized to effective body mass, and expressed as kcal/h/kgEff.Mass. Fat oxidation (FO) and carbohydrate oxidation (CHO) were calculated as FO = 1.69 x VO2 – 1.69 x VCO2 and CHO = 4.57 x VCO2– 3.23 x VO2 and expressed as $g/d/kg^{Eff.Mass}$. References for the equations used can be found in (41).

Activity and position were monitored simultaneously with the collection of the calorimetry data using XYZ beam arrays with a beam spacing of 0.25 cm. Food and water intakes were measured while calorimetric data were sampled.

Flow cytometry

For WAT endothelial cells enumeration, a single-cell suspension containing the stromal cell fraction was prepared from WAT as previously described (*42*) and washed in staining buffer (0.2% BSA and 5 mM glucose in PBS). Hematopoietic cells were excluded using Pacific-blue rat anti-mouse CD45 (BioLegend; clone 30-F11) and rat anti-mouse Ter119 (BioLegend; clone TER-119). Endothelial cells were then identified with PE-rat anti-mouse CD31 (BioLegend clone 390) and biotin rat anti-mouse Pan-endothelial cell Antigen (BioLegend clone MECA-32) with APC/cy7 Streptavidin (BioLegend #405208).

Immune cells infiltrates in WAT and Liver were identified by exclusion of erythrocytes (using Pacific blue rat anti-mouse Ter119 (BioLegend; clone TER-119)) and marking of leukocytes using PE-rat anti-mouse CD45 (BD Bioscience clone 30-F11).

Liver Senescent endothelial cells were quantified as follows: a liver sample was homogenized to a single cell suspension and CD146+ endothelial cells were captured on CD146 (LSEC) microbeads (Miltenyi Biotec) according to the manufacturer instructions. Cells were pretreated with 300µM chloroquine for 20 min in fresh cell culture medium at 37C°, 5% CO2. The SA-β-gal substrate C12FDG (Thermofisher #D2893) was then added to a final concentration of 33µM and samples were incubated for 40min at 37C°, 5% CO2. Cells were centrifuged at 1500 RPM, washed twice with PBS and resuspended in 100µl of staining solution containing Pacific-blue rat anti-mouse CD45 (BioLegend; clone 30-F11) and rat anti- mouse Ter119 (BioLegend; clone TER-119), PE-rat anti-mouse CD31 (BioLegend clone 390). Samples were incubated for 30 min, washed and processed for flow cytometry.

Flow cytometry was performed on a MACS Quant Analyzer (Miltenyi), and data analyzed using FlowJo version 10.

Oxygen consumption assay

Mitochondrial oxygen consumption rates by isolated skeletal muscle fibers were measured ex-vivo using Agilent Seahorse XF24 Analyzer. Skeletal muscles (Tibialis Anterior and Extensor Digitorum Longus) were ressected from the specified experimental groups of mice. Myofibers were isolated by first, incubating the muscle tissue in 0.2% Collagenase type I in DMEM (Dulbecco's modified Eagle's mediums, high glucose, supplemented with L-glutamine and Sodium pyruvate- Biological Industries, #01-055- 1A) for 10 min at 37 °C. Myofibers were then released through gentle flushing of the muscle using a 1 ml pipette with a large bore to limit damage to the fibers. Single myofibers were then seeded on to a XF24 cell culture microplate pre-coated with 3 µl of Matrigel (Corning, #354230) in DMEM medium and incubated at 37 °C for 1 h at 5% CO2. Medium was replaced with pre-warmed assay medium (Agilent Technologies, #103334-100) and equilibrated for 1 hr at 37 °C. Meanwhile, Agilent Seahorse XF Assay Cartridge was loaded with Oligomycin (1 µM), FCCP (1 µM) and Rotenone/AntimycinA (5 µM) in Ports A, B and C respectively. During the equilibration period, the compound loaded cartridge was calibrated as recommended by the manufacturer. Following

calibration, the calibration plate was replaced with the plate containing the fibers and readings were recorded to calculate OCR. OCR was normalized to the total protein content of muscle fibers that was measured using Bradford assay (BioRad)

Rotarod assay
Rotarod assay was performed by placing each mouse on a horizontal rod, which rotates with an acceleration rate of 5 rounds per minute (rpm) to achieve a maximum of 40 rpm in 99 seconds. Time before falling from the rod is recorded (with a cut-off time of 4 min). Each mouse underwent 3 consecutive trials separated by a 20 mn resting interval. Measures from the last 2 trials are averaged to determine time before falling.

µCT imaging and bone morphometry
Bones were harvested and immersion-fixed in 2% paraformaldehyde solution until scanning. To prevent their eventual displacement during the scan, the samples were wrapped into moisturized melamine foam and placed into a cylindrical sample holder. Bones were scanned in Bruker® Skyscan 1172 X-ray microCT system with 50kV acceleration voltage and 200µA current on the X-ray source. No filter was applied. The scanning was done for 360 degrees' rotation with rotation step of 0.1 degree resulting in 3600 projections. Each projection was 4000x2672 pixels with resolution of each pixel of 2.98µm. Reconstruction was done with Bruker® reconstruction software NRecon. Prior to reconstruction, each dataset was corrected for thermal shifts as well as misalignment according to the manufacturer's protocol (Bruker microCT).
Each dataset was realigned and correspondingly resliced in ImageJ software in order to achieve same orientation of the tibia. Afterwards, the tibia segment of 200 virtual sections was delineated as volume of interest (VOI) for further bone morphometry analysis. The proximal limit of the VOI was located approximately 0.5cm (≈170 layers) below the most distal ossified part of the tibias epiphyseal plate. Bone morphometry analysis was conducted using CTAn Software (Bruker microCT) according to the manufacturer's instructionsX-ray micrograph.

Transmission electron microscopy
Muscle and liver tissue were cut into 3 mm slices and fixed in 2% paraformaldehyde, 2.5% Glutaraldeyde in 0.1M Cacodylate buffer (pH 7.4) overnight at room temperature. Tissues were then rinsed 4 times, 10 minutes each, in cacodylate buffer and post fixed and stained with 1% osmium tetroxide, 1.5% potassium ferricyanide in 0.1M cacodylate buffer for 1 hour. Tissues were then washed 4 times in cacodylate buffer followed by dehydration in increasing concentrations of ethanol (30%, 50%, 70%, 80%, 90%, 95%) for 10 minutes each step followed by 100% anhydrous ethanol 3 times, 20 minutes each, and propylene oxide 2 times, 10 minutes each. Following dehydration, tissues were infiltrated with increasing concentrations of Agar 100 resin in propylene oxide, consisting of 25, 50, 75, and 100% resin for 16 hours each step. The tissues were then embedded in fresh resin and let polymerize in an oven at 600C for 48 hours.
Embedded tissues in blocks were sectioned with a diamond knife on a Leica Reichert Ultracut S microtome and ultrathin sections (80nm) were collected onto 200 Mesh, thin bar copper grids. The sections on grids were sequentially stained with Uranyl acetate for

5 minutes and Lead citrate for 2 minutes and viewed with Jeol, TEM 1400Plus, Japan with charge-coupled device camera (Gatan Orius SC600). Multiple sections derived from 3 mice of each group were examined. The most representative images are included in Supplemental figures S18 and S19.

Measurements of Kyphosis Index:
Radiography imaging of sedated mice immobilized on a radiographic table was done using OEC 9900 Elite (General Electric) in Roentgen mode. Mice were radiographed at the age of 12 mo and, again, at the age of 24 mo. Kyphosis index (KI) was calculated as the distance between the caudal margin of the last cervical vertebra to the caudal margin of the sixth lumbar vertebra (usually corresponding to the cranial border of the wing of the ilium) divided by a line perpendicular to this from the dorsal edge of the vertebra at the point of greatest curvature, as previously described (43). Care was taken to avoid overextension or flexion of limbs.

Statistical analysis
For the statistical analysis of survival and tumor incidence, Chi square log-rank (Mantel-Cox) test was used. For comparison between two groups, Student's t test was used. Comparisons between multiple groups with one variable were calculated by one- way ANOVA with Tukey post-test. Comparisons between multiple groups with two variables were calculated by two-way ANOVA with Bonferonni post-tests. Comparisons between multiple groups with not normal distribution were calculated by ANOVA non- parametric test (Kruskal-Wallis test and Dunn's Multiple Comparison post-Test). p values assumed two-tailed distribution and unequal variances (*, $P < 0.05$; **, $P < 0.01$; ***, $P < 0.001$). Statistical information relevant to individual experiments is detailed in the figure legends. GraphPad Prism 7 software was used for statistical analysis. The investigators were not blinded during group allocation, the experiment, or when assessing the outcome.
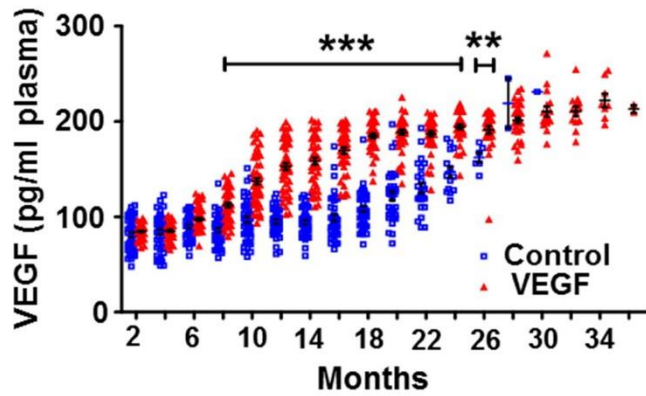
Fig. S1.

Plasma VEGF protein levels in female control and VEGF mice. VEGF levels were determined at progressive ages with a VEGF-A-specific ELISA. *n=50 mice per group*. Values measured in Control and VEGF male mice were significantly different between 8 to 26 months of age.

Statistical analysis. Each dot represents a mouse. p values derived from Two-way ANOVA with Bonferroni post-tests. Values are mean +/-SEM.

p values indicated as * <0.05; **<0.01; *** <0.001. p values > 0.05 are not indicated
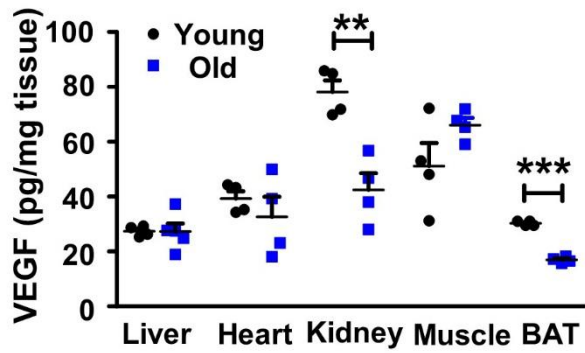
Fig. S2.

VEGF levels in peripheral organs of naïve mice. VEGF in lysates of the indicated organs prepared from young (2-4 months old) and old (20-24 months old) mice were determined with a VEGF ELISA. *n=4 mice per organ*.

Statistical analysis. Each dot represents a mouse. p values are derived from two-tailed Student's t test. Values are mean +/-SEM.

p values indicated as * <0.05; **<0.01; *** <0.001. p values > 0.05 are not indicated
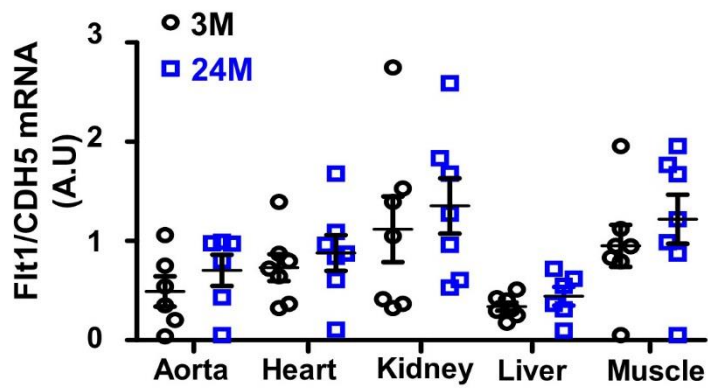
Fig. S3.

Age-related VEGFR1 (Flt1) expression. Relative levels of Flt1 expression in the indicated organs and ages, as determined by qPCR with primers detecting mRNAs encoding the full-length receptor. Levels were standardized to the level of mRNAs encoding the pan-endothelial marker CDH5. *n=7 mice per group*

Statistical analysis. Each dot represents a mouse. p values are derived from two-tailed Student's t test. Values are mean +/-SEM.

p values indicated as * <0.05; **<0.01; *** <0.001. p values > 0.05 are not indicated
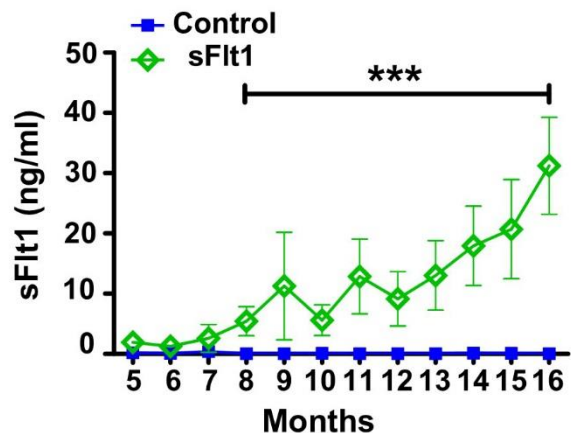
Fig. S4.

Circulating levels of transgenic sFlt1 induced in a VE-Cadherin::sFlt1 bi-transgenic system. Monthly monitoring with a human sFlt1 ELISA of plasma sFlt1 levels induced in the sFlt1 inducible system (see 'Methods' for details). Significantly higher levels of sFlt1 are measured from 8 months and onwards at each time point.

Statistical analysis: Each dot represents the mean concentration measured in the blood of *5 mice per group*. p values are derived from Two-way ANOVA with Bonferroni post- tests. Values are mean +/-SEM. p values indicated as * <0.05; **<0.01; *** <0.001. p values > 0.05 are not indicated
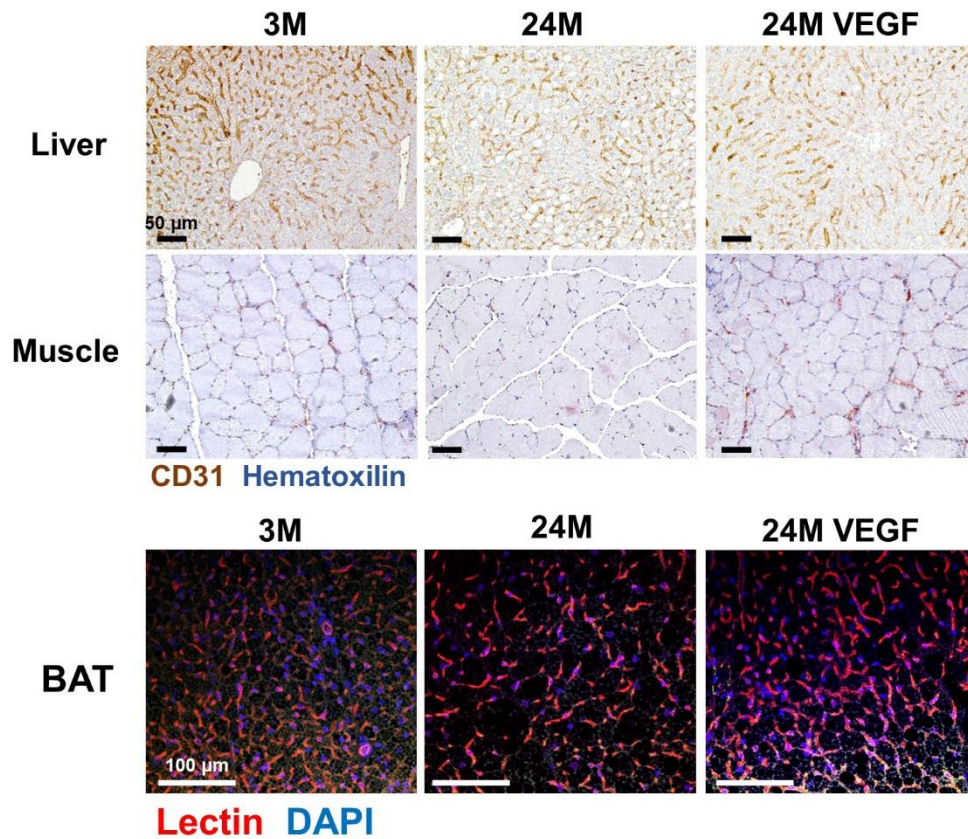
Fig. S5.

Representative images of sections immunostained for blood vessels. Sections of the indicated organs obtained from young (2-4 months old) and old (20-24 months old) mice were stained for the EC-specific marker CD31 or lectin.
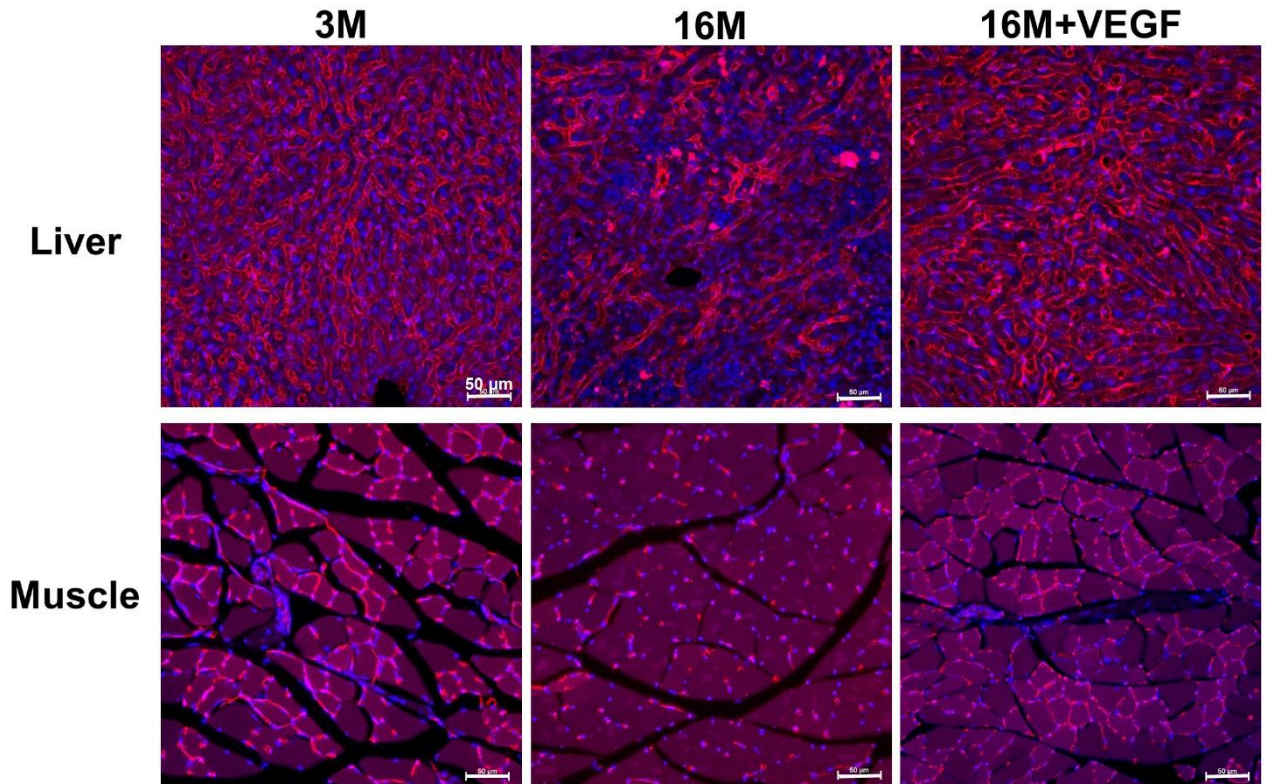
Fig. S6

Visualization of perfused vessels in liver and muscle. Representative images of tissue sections used for calculating the relative area occupied by perfused vessels presented in **Fig. 1I**. Perfused vessels are highlighted by red fluorescence and nuclei by DAPI staining (see Methods for details).
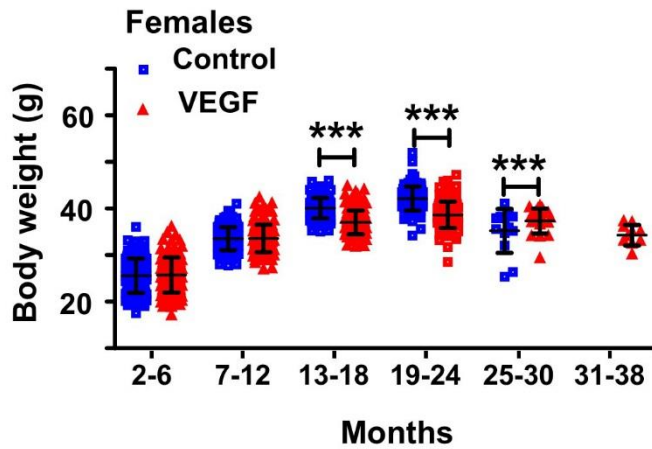
Fig. S7

Body weights of female mice. Mice weighed monthly were divided for presentation in age groups of 5 to 6 months each. *n>8 per each age group*.

Statistical analysis: Each dot represents a mouse. p values derived from two-tailed unpaired Student's t test. Values are mean +/-SEM. p values indicated as * <0.05; **<0.01; *** <0.001. p values > 0.05 are not indicated
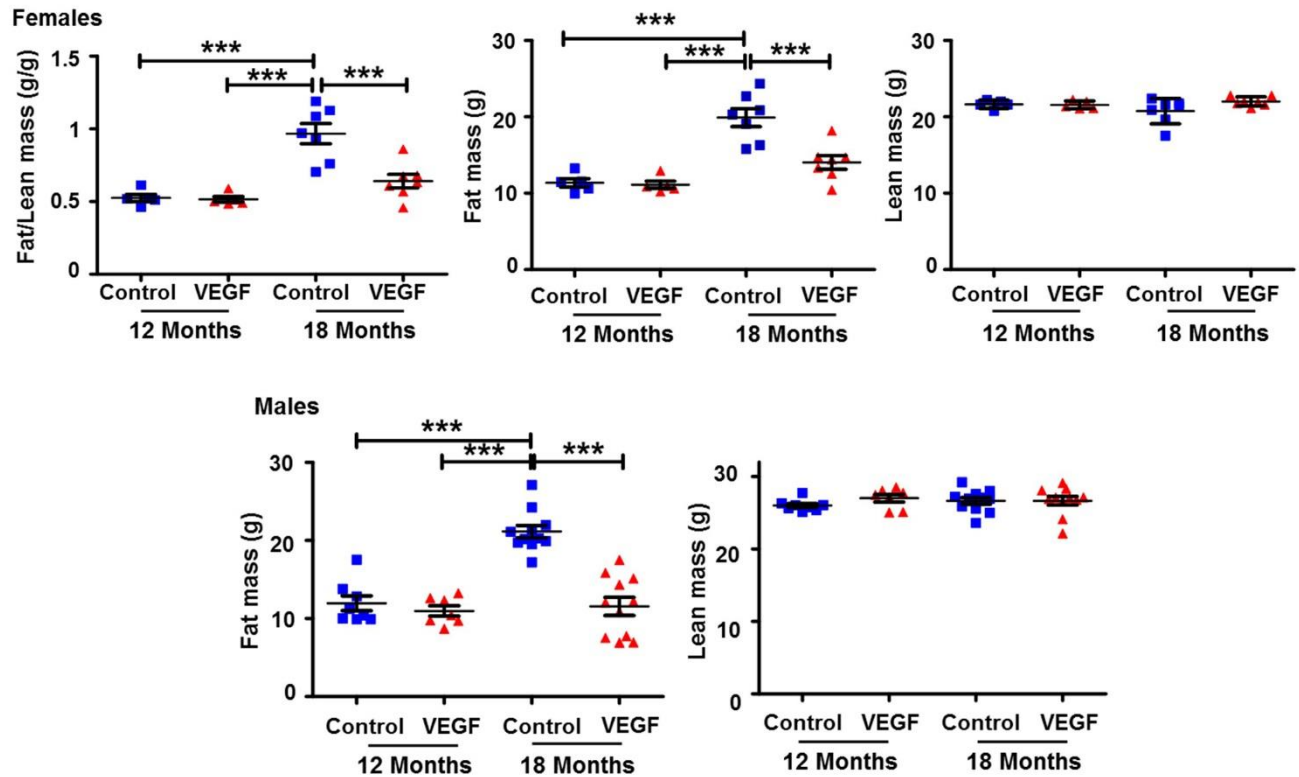
Fig. S8 Fat and lean body masses

Upper panel – Fat/lean body mass (left graph) of female control and VEGF mice was calculated at the indicated ages on the basis of Echo-MRI measurements. Fat and lean masses are detailed for each mouse in middle and right graphs respectively.

Lower panel **-** Fat and lean masses measured by Echo-MRI in control and VEGF male mice at the indicated ages.

Each dot represents the average of 2 measurements per mouse. *11 >n>5 mice per group*.
Statistical analysis: Each dot represents a mouse. p values are derived from One-way ANOVA with Tukey post-tests. Values are mean +/-SEM.
p values indicated as * <0.05; **<0.01; *** <0.001. p values > 0.05 are not indicated
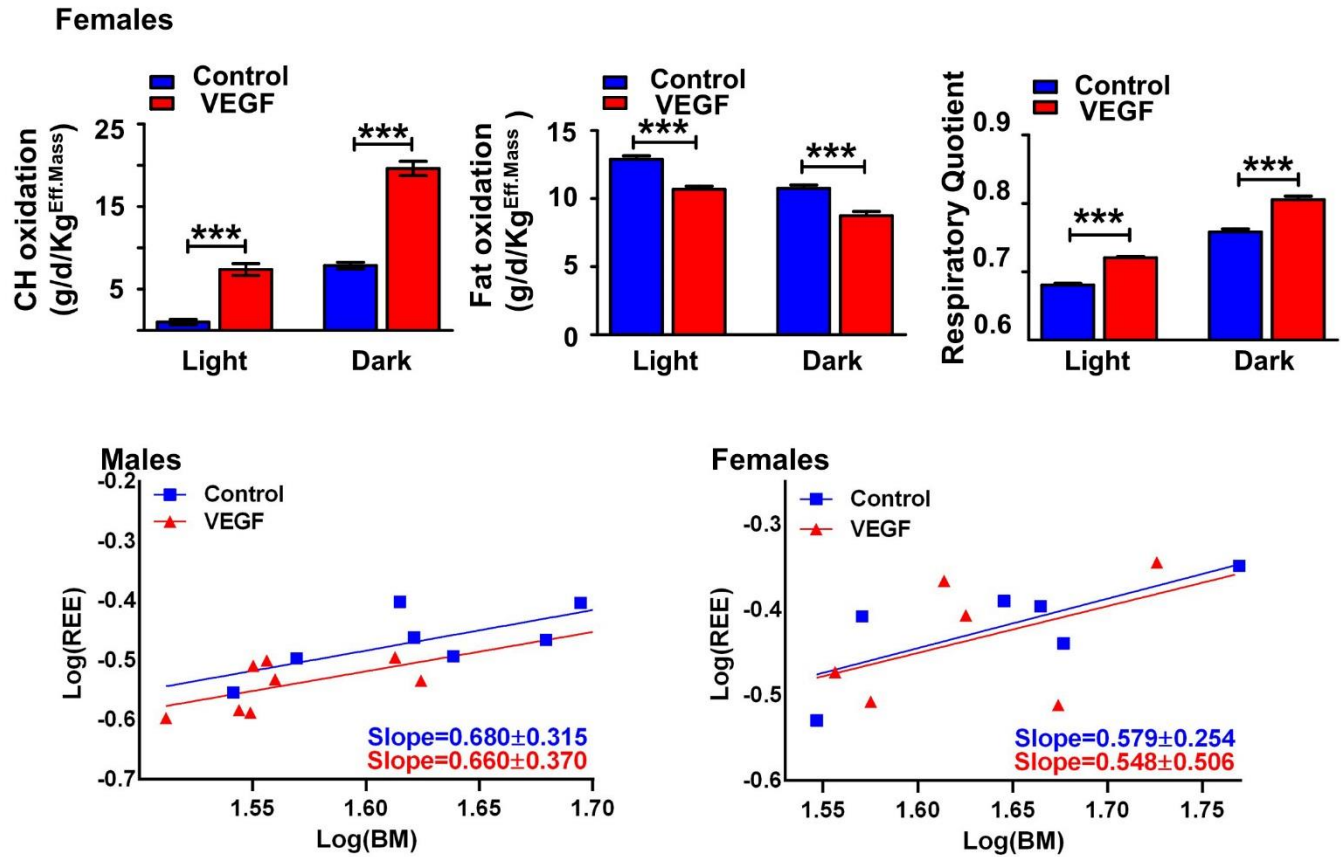
Fig. S9

Carbohydrate oxidation, fat oxidation and Respiratory Quotient in female mice upper panel:16 months old female mice were individually housed in metabolic cages and the indicated metabolic parameters were monitors in both light and dark phases
lower panel: ANCOVA analysis- allometric regression graphs indicating no significant differences in slopes between control and VEGF mice (p value for Males: 0.9686; p value for Females: 0.9556).
8> n>6 for each group
Statistical analysis:
p values are derived from two-tailed unpaired Student's t test. Values are mean +/-SEM. p values indicated as * <0.05; **<0.01; *** <0.001. p values > 0.05 are not indicated
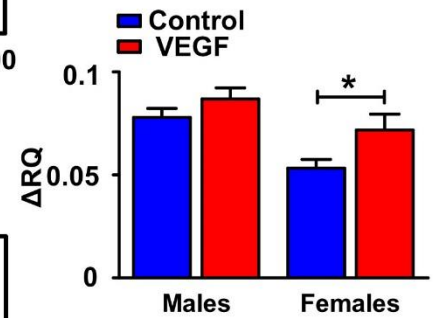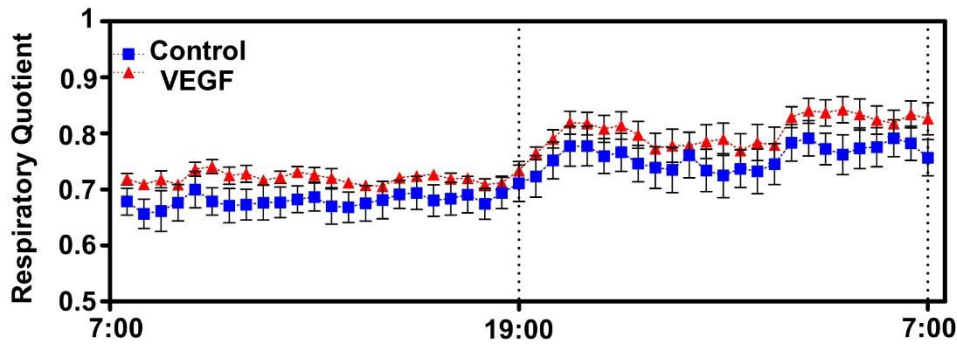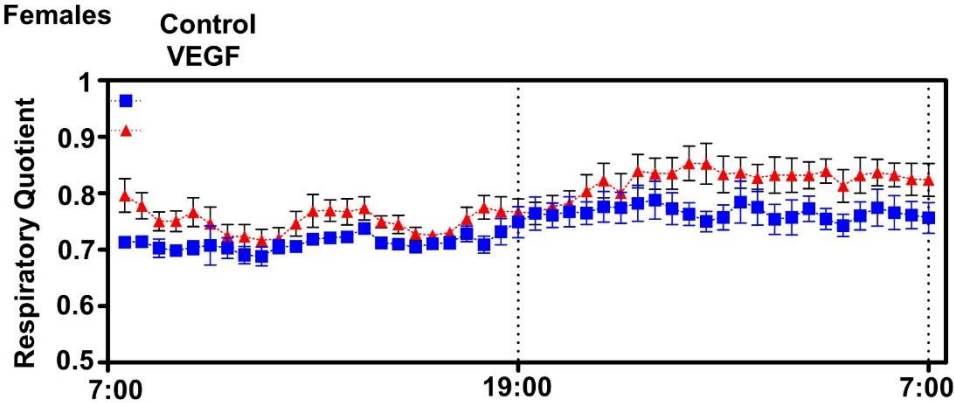
Fig. S10

Circadian dynamics of RQ changes in 16 months old control- and VEGF mice. Left: Half-hourly changes in RQ in the course of a 12h light/12h dark cycle [mice used are those for which averaged RQ values for the respective light and dark periods were presented in Figures 2D (males) and S10 (females)].

Right: The extent by which RQ during the metabolically active dark period is higher in VEGF mice compared to control mice (ΔRQ), indicating a significant increase in female mice (p<0.05). *8> n>6 for each group*

Statistical analysis:

p values are derived from two-tailed unpaired Student's t test. Values are mean +/-SEM. p values indicated as * <0.05; **<0.01; *** <0.001. p values > 0.05 are not indicated
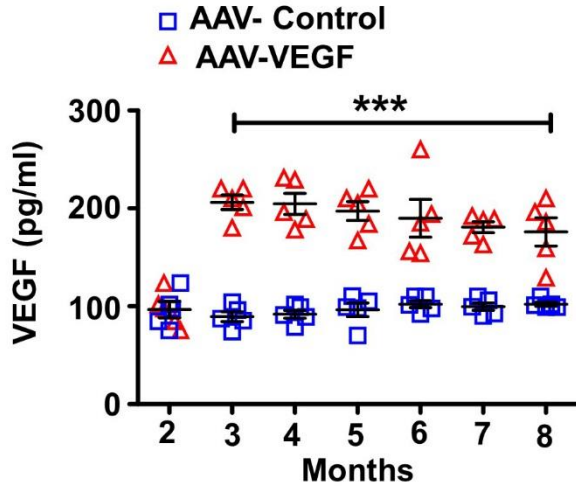
Fig. S11

Circulating VEGF levels after AAV-VEGF infection. Wild-type mice were infected with a
low-titer AAV-VEGF165 virus (or with control virus) at the age of 2 months.
Plasma VEGF levels were measured monthly using a VEGF ELISA (mice with lower levels of
VEGF were reinjected at 5 months). Significant higher levels at each time point are observed
from 3 months and onward. *n=5 mice per group*
Statistical analysis: Each dot represents a mouse. p values are derived from Two-way ANOVA
with Bonferroni post-tests. Values are mean +/-SEM. p values indicated as * <0.05; **<0.01;
*** <0.001. p values > 0.05 are not indicated
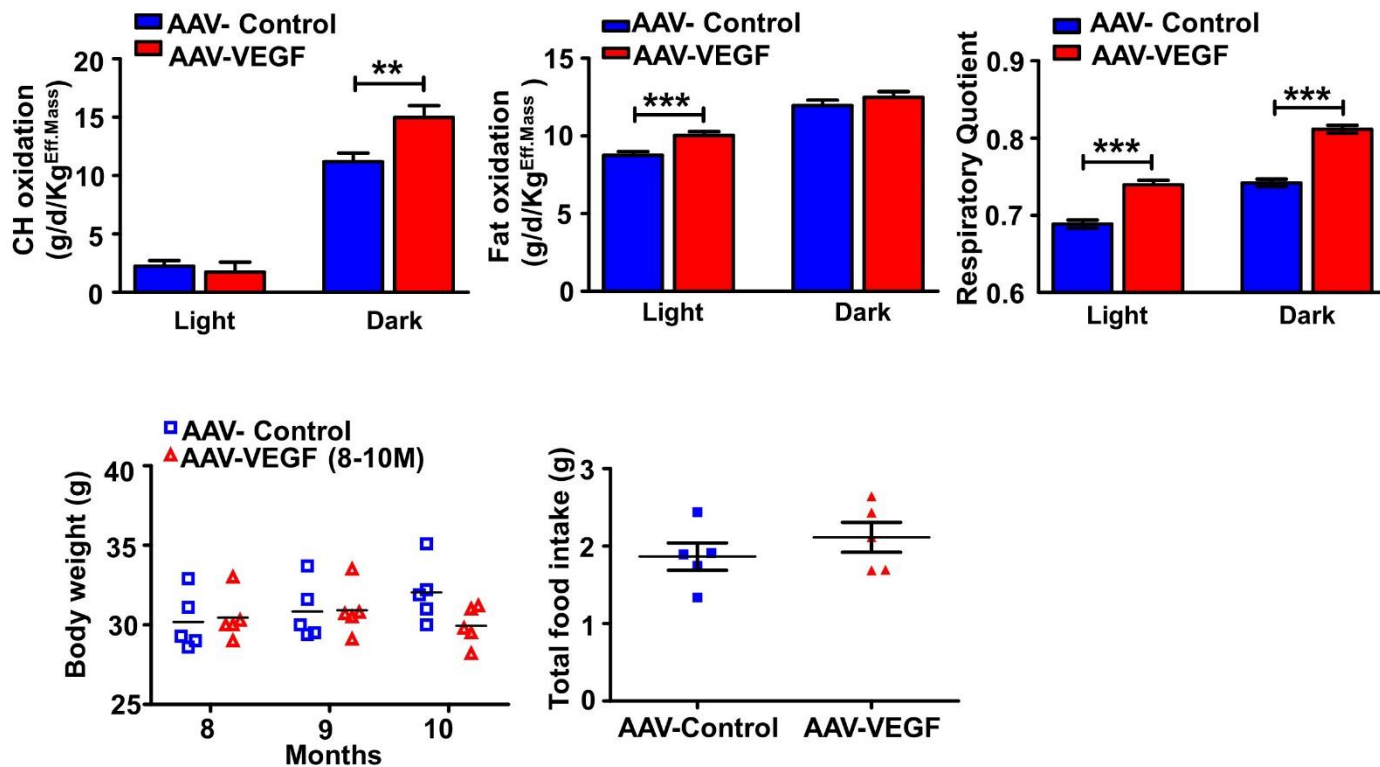
Fig. S12

Circadian changes in carbohydrate and fat oxidation and in RQ (upper panel): 8 months old mice were infected with a low titer of AAV-VEGF164 in parallel to control mice infected with the same titer of control AAV vector (*n=5 for each group of mice*). Mice in metabolic cages were analyzed upon reaching the age of 10 months.

Body weight and total food intake (lower panel) were measured in the same mice used in metabolic cages analysis. Each dot represents a mouse.

Statistical analysis: p values are derived from two-tailed unpaired Student's t test. Values are mean +/-SEM. p values indicated as * <0.05; **<0.01; *** <0.001. p values > 0.05 are not indicated
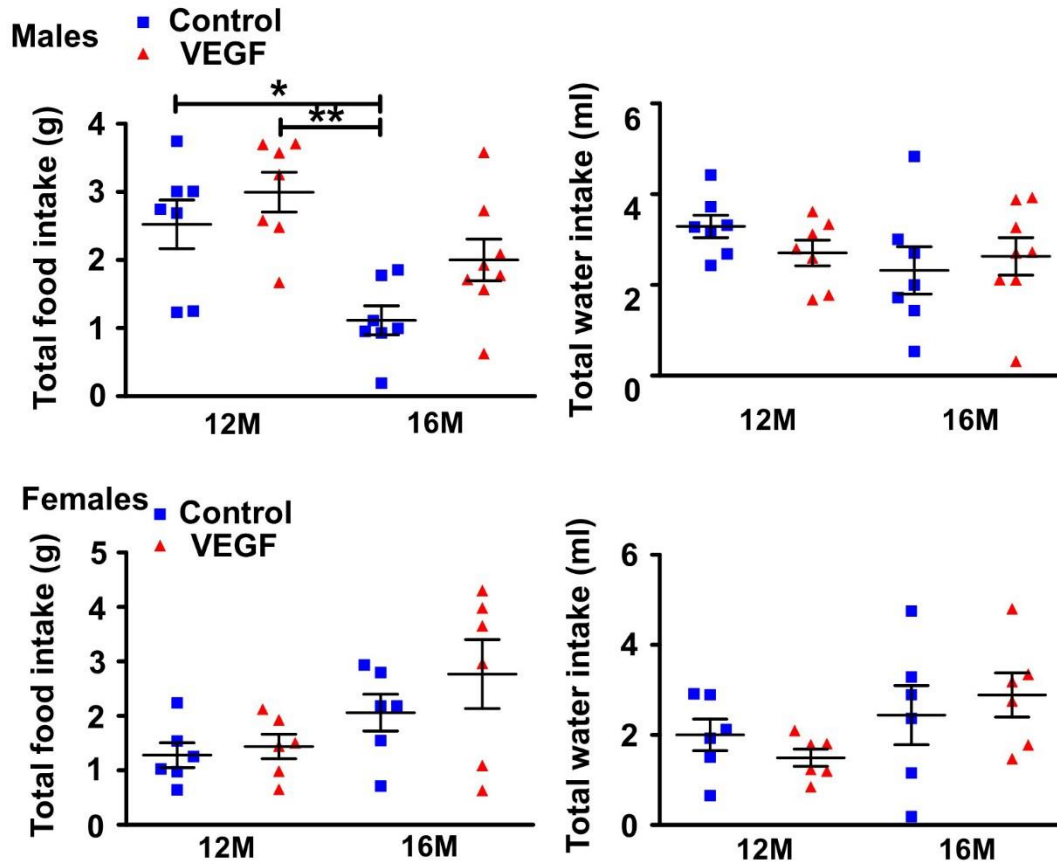
Fig. S13

Food and water intakes measured in 16 months old control and VEGF mice. Total food and water intakes and voluntary physical activity were measured as described under 'Methods' in 12 months old mice and in 16 months old mice used for measuring the metabolic parameters presented in Figures 2D, S10 and S11.

Statistical analysis: Each dot represents a mouse**.** p values derived from one-way ANOVA nonparametric test (Kruskal-Wallis test and Dunn's Multiple Comparison post- Test). Values are mean +/-SEM. p values indicated as * <0.05; **<0.01; *** <0.001. p values > 0.05 are not indicated

16M Males
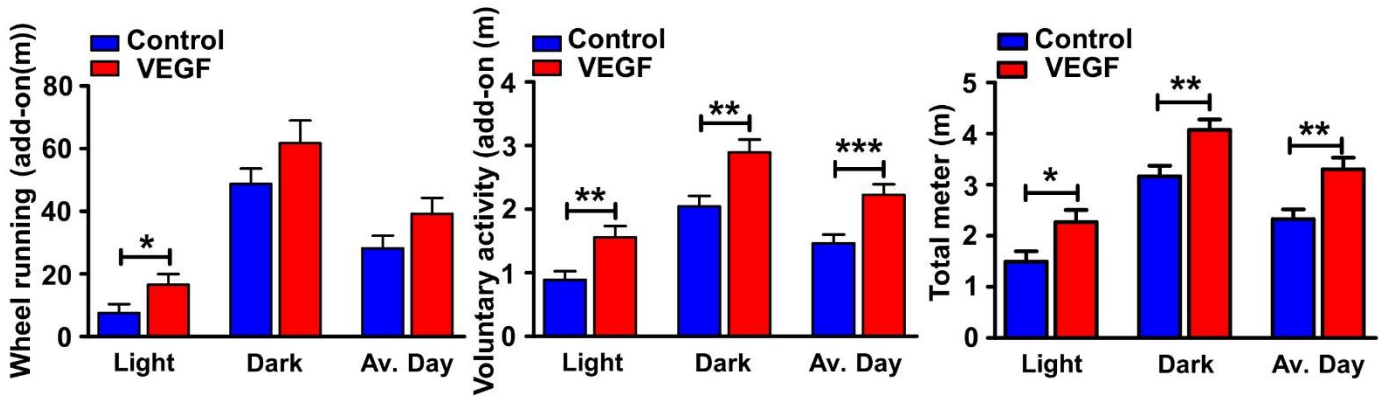
16M Females
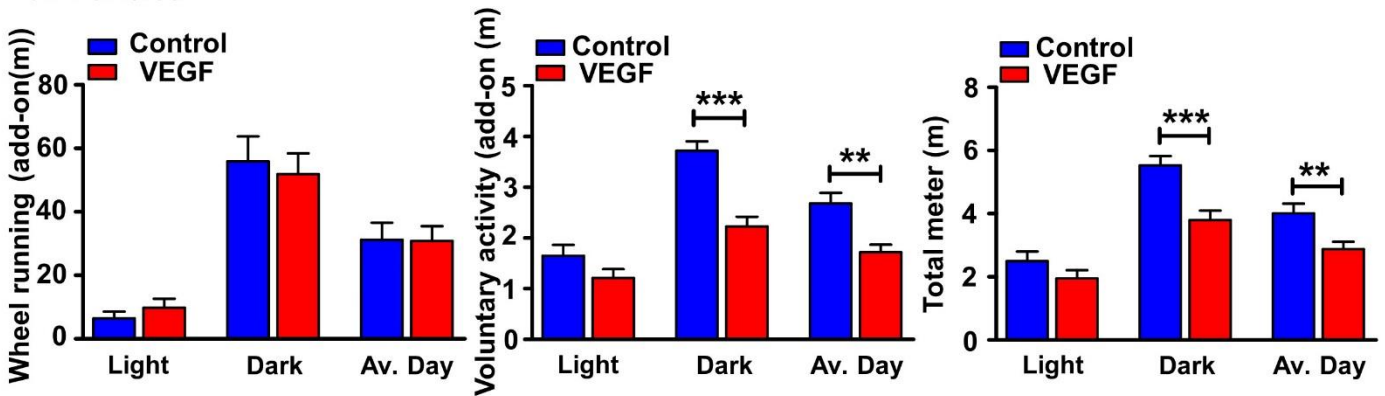
Fig. S14

Physical activity of 16 Mo male (upper panel) and female (lower panel) mice Wheel running, voluntary activity and total distance covered during active and resting periods were measured in a 24 hrs cycle of stay in metabolic cages. *8>n>6 mice per group*

Statistical analysis: p values are derived from two-tailed unpaired Student's t test. Values are mean +/-SEM. p values indicated as * <0.05; **<0.01; *** <0.001. p values > 0.05 are not indicated
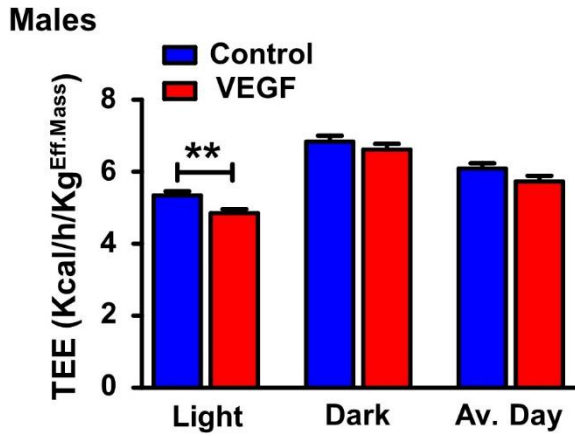
Fig. S15

Total energy expenditure (TEE) by 12M old control and VEGF male mice normalized to effective body mass) measured by indirect calorimetry. *n=7 mice per group*
Statistical analysis: p values are derived from two-tailed unpaired Student's t test. Values are mean +/-SEM. p values indicated as * <0.05; **<0.01; *** <0.001. p values >
0.05 are not indicated.
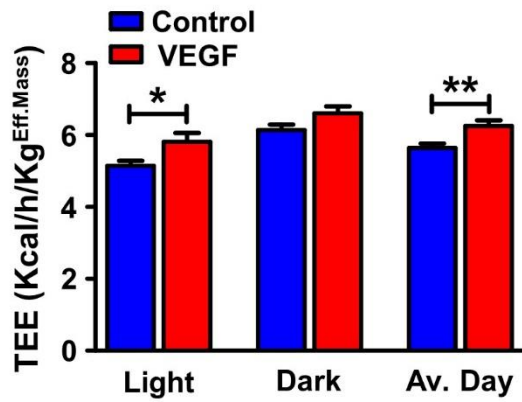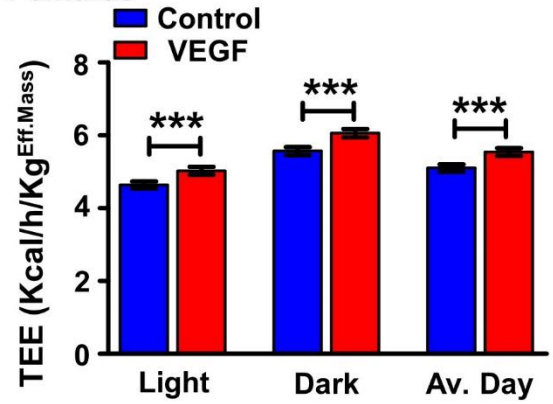
Fig. S16
Total energy expenditure (TEE) in12 and 16 months old female mice. TEE was measured by indirect calorimetry. Values shown were normalized to effective body mass. *n=6 for each group*
Statistical analysis: p values derived from two-tailed unpaired Student's t test. Values are mean +/-SEM. p values indicated as * <0.05; **<0.01; *** <0.001. p values > 0.05 are not indicated
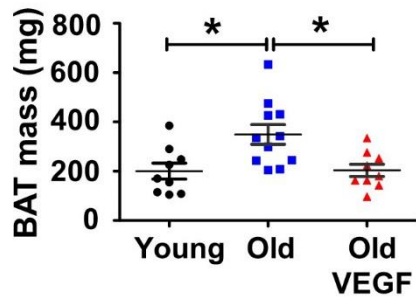
Fig. S17

BAT mass in young and old mice.Whole interscapular brown adipose tissue of young (3 mo) and old male and female mice (24 mo) was resected and weighted. *n>8 in each group*
Statistical analysis: p values derived from One-way ANOVA with Tukey post-tests. Values are mean +/-SEM. p values indicated as * <0.05; **<0.01; *** <0.001. p values >
0.05 are not indicated
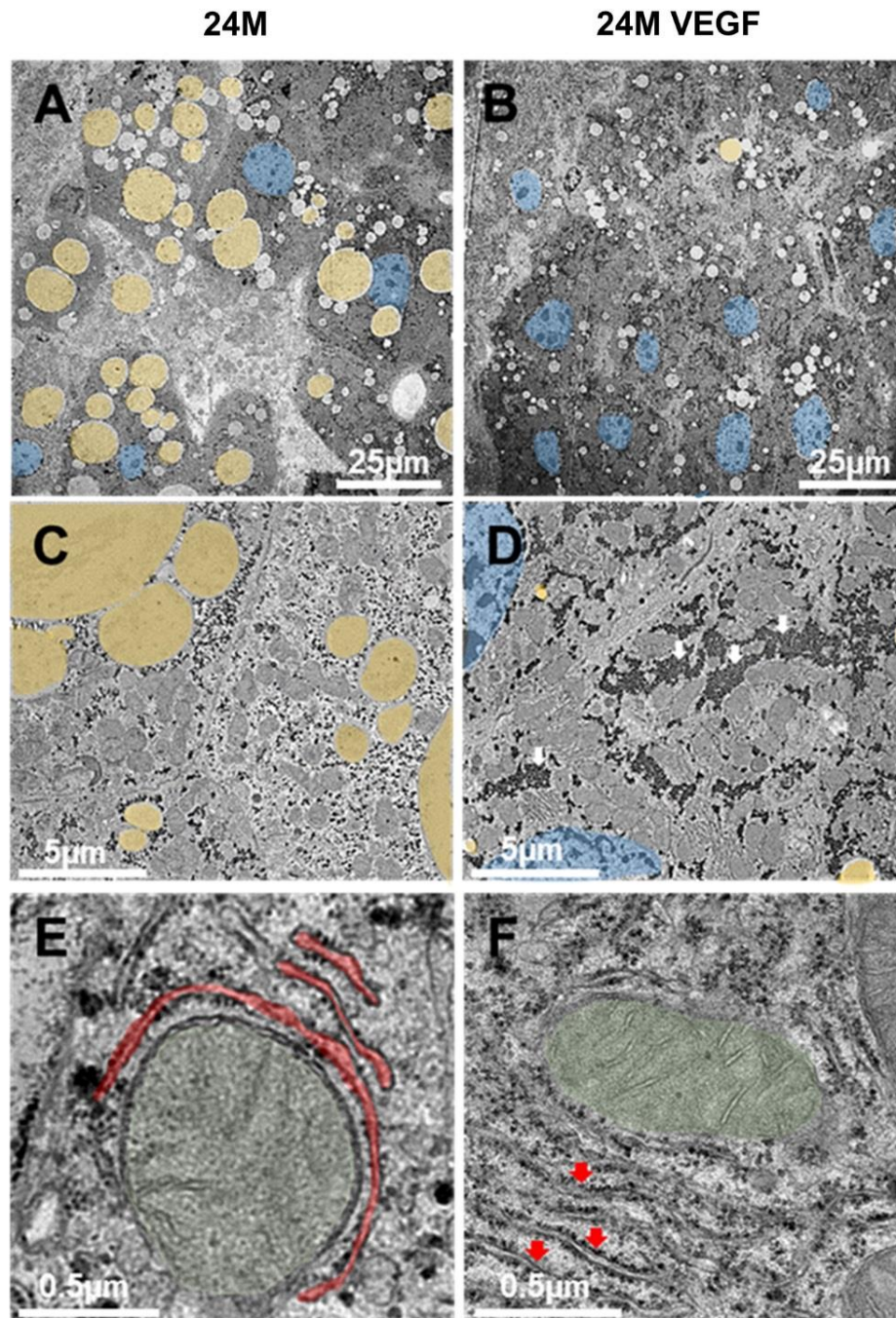
Fig. S18

Representative Electron microscopy images of liver sections from old control and VEGF mice. Pseudocolors highlight: (A, B) lipid droplets larger than 1 µm (yellow), (A, B, D) hepatocytes nuclei (blue); (E) swollen and ribosomes-deprived endoplamic reticulum (red). Large mitochondria with disorganized cristae were observed in Old control mice (E, green). White arrows indicate glycogen deposition observed in Old VEGF mice (D). Red arrows indicate ribosomes-decorated endoplasmic reticulum observed in Old VEGF mice (F). Bars are as indicated
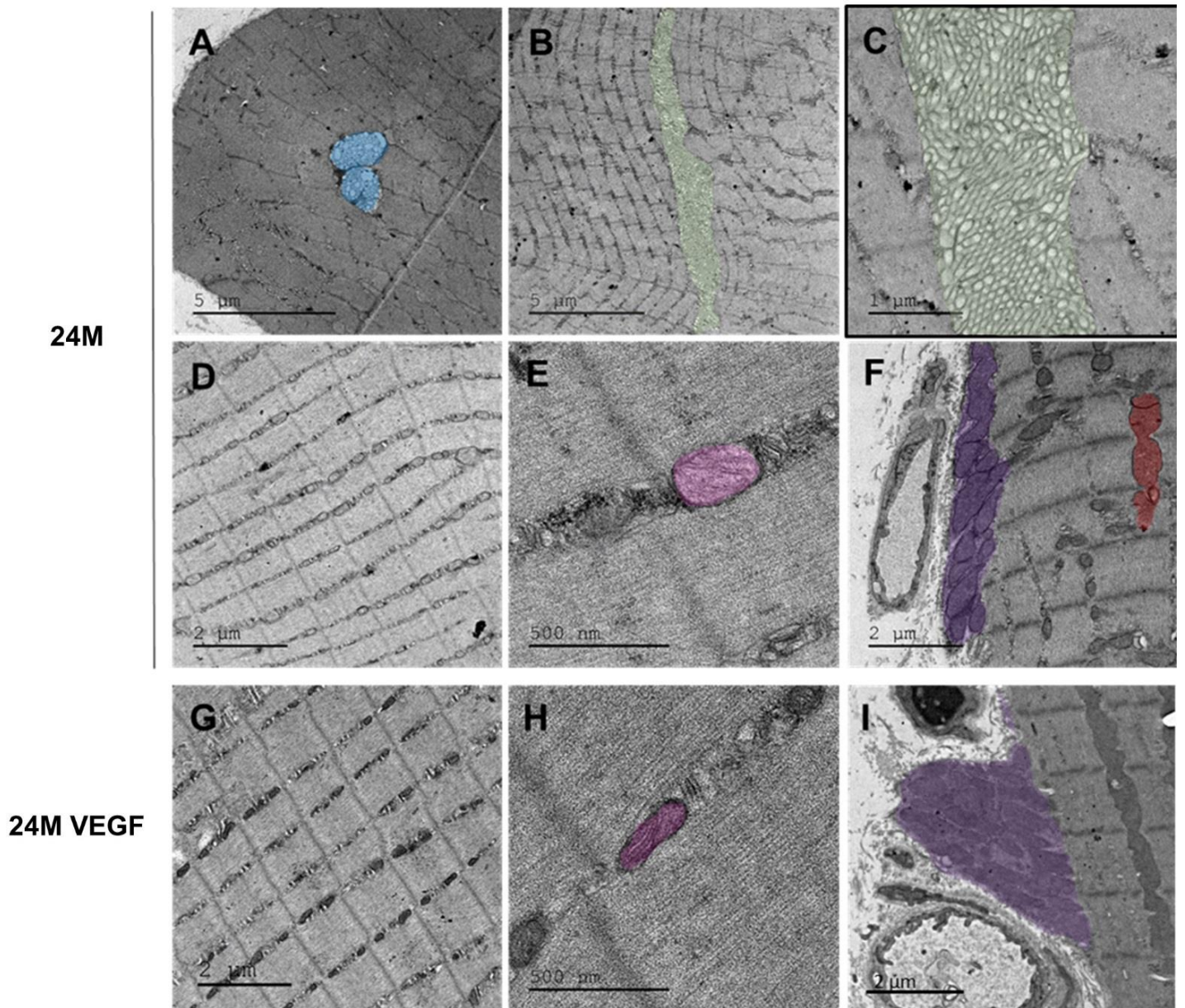
Fig. S19

Representative electron microscopy images of hind limb muscle sections from old control and VEGF mice (24 months old). Pseudocolors highlight: (A) ectopic multivesicular bodies (blue); (B, C) tubular aggregates in the sarcoplasmic reticulum (green); (E, H) interfibrillar mitochondria (pink) that appeared swollen in old control muscle; (G, I) sub-sarcollema mitochondria (violet) that were more numerous in Old VEGF mice.

Table S1.

Genotype, lifespan and presence of tumors at the time of death for all female mice used in survival studies.

Horizontal red lines separate different litters.

Genotype: D- mice harboring only the driver transgene; R- mice harboring only the VEGF responder transgene; VEGF- double transgenic mice harboring both driver and responder transgenes.

Lifespan: Mice were euthanized when clinical signs suggested death within 24 hours or, in some cases, died naturally.

Censored mice (0): Reasons for censoring the indicated mice were – V1 and V5 suffered from malocclusion impairing normal weight gain; V3, V6, V21, V22, V23 and V19 presented ear/skin dermatitis resistant to antibiotics treatment; V10, V13, V4 and V20 presented severe fight injuries; V2 suffered from vaginal tissue prolapse. Otherwise, these mice did not present any clinical sign suggesting imminent death.

Tumors: presence of apparent neoplastic lesions at the time of sacrifice and the affected organs

Mouse ID	Gene	Date of birth	Date of death	Age at death (Days)	Age at death (Months)	Censored (0) Included (1)	Neoplastic lesion in indicated organ
V1	VEGF	01/02/15	04/11/15	273	8.97	0	0
C1	D	01/02/15	02/04/16	421	13.84	1	0
C2	R	01/02/15	04/06/16	483	15.88	1	0
V4	VEGF	01/02/15	12/11/16	641	21.07	0	0
V16	VEGF	01/02/15	22/10/17	981	32.25	1	WAT
C4	R	02/02/15	27/08/16	565	18.57	1	Liver, WAT
C10	D	02/02/15	07/01/17	695	22.85	1	Skin, Spleen
C13	D	02/02/15	13/02/17	731	24.03	1	Spleen, Liver
V7	VEGF	02/02/15	14/06/17	852	28.01	1	0
V15	VEGF	02/02/15	28/09/17	956	31.43	1	0
C3	D	28/02/15	06/08/16	518	17.03	1	Skin, Liver
C7	R	28/02/15	17/10/16	589	19.36	1	0
C8	R	28/02/15	11/12/16	643	21.14	1	0
V6	VEGF	28/02/15	10/04/17	762	25.05	0	0
V17	VEGF	28/02/15	05/11/17	967	31.79	1	0
V3	VEGF	01/03/15	01/08/16	510	16.77	0	0
C5	D	01/03/15	09/09/16	548	18.01	1	Skin
C6	R	01/03/15	04/10/16	573	18.84	1	0
V9	VEGF	01/03/15	18/06/17	827	27.19	1	WAT

V18	VEGF	01/03/15	09/12/17	998	32.81	1	0
V2	VEGF	09/03/15	19/06/16	460	15.12	0	Spleen
C9	R	09/03/15	05/01/17	656	21.56	1	Skin
V8	VEGF	09/03/15	14/06/17	815	26.79	1	Liver
V11	VEGF	09/03/15	24/08/17	885	29.09	1	0
V12	VEGF	09/03/15	06/09/17	897	29.49	1	WAT
V14	VEGF	09/03/15	22/09/17	913	30.01	1	Spleen
C12	D	08/03/16	21/01/17	313	10.29	1	0
C18	D	08/03/16	27/10/17	589	19.36	1	0
V19	VEGF	08/03/16	03/01/18	655	21.53	0	0
C23	R	08/03/16	06/01/18	658	21.63	1	0
C42	D	08/03/16	11/06/18	813	26.73	1	Skin, Spleen
V31	VEGF	08/03/16	21/10/18	943	31.00	1	0
V50	VEGF	08/03/16	07/04/19	1109	36.46	1	0
C11	D	10/03/16	16/01/17	306	10.06	1	Skin
C22	D	10/03/16	27/12/17	647	21.27	1	Skin
C26	R	10/03/16	23/01/18	673	22.12	1	WAT, Skin
V33	VEGF	10/03/16	23/10/18	943	31.00	1	0
V47	VEGF	10/03/16	11/03/19	1081	35.54	1	0
V49	VEGF	10/03/16	03/04/19	1103	36.26	1	0
C14	R	15/03/16	26/02/17	341	11.21	1	0
C16	D	15/03/16	01/06/17	436	14.33	1	0
C21	D	15/03/16	01/12/17	616	20.25	1	Spleen, Liver
C27	R	15/03/16	03/02/18	678	22.29	1	Liver, Lung, WAT
V20	VEGF	15/03/16	20/02/18	695	22.85	0	0
	VEGF	15/03/16	28/10/18	943	31.00	1	Ovary
V41	VEGF	15/03/16	05/01/19	1010	33.20	1	0
C15	R	18/03/16	21/03/17	363	11.93	1	Spleen, Skin
C19	D	18/03/16	06/11/17	588	19.33	1	Spleen, Skin
C29	R	18/03/16	28/02/18	700	23.01	1	Spleen, Liver , Lung
C33	D	18/03/16	28/03/18	730	24.00	1	Liver
V24	VEGF	18/03/16	21/08/18	873	28.70	1	0
V32	VEGF	18/03/16	22/10/18	934	30.70	1	Intestine
V39	VEGF	18/03/16	30/11/18	972	31.95	1	0
V5	VEGF	20/03/16	27/03/17	367	12.06	0	0

C17	D	20/03/16	30/06/17	460	15.12	1	Spleen, Liver
C20	D	20/03/16	10/11/17	590	19.40	1	Spleen, Liver, BAT
C30	R	20/03/16	01/03/18	701	23.04	1	Skin, WAT
C34	R	20/03/16	03/04/18	733	24.10	1	Spleen, Liver, WAT
C38	D	20/03/16	30/04/18	760	24.98	1	Liver, Lung
V26	VEGF	20/03/16	04/10/18	914	30.05	1	Liver
V43	VEGF	20/03/16	04/02/19	1034	33.99	1	WAT, Liver
V48	VEGF	20/03/16	16/03/19	1076	35.37	1	0
V10	VEGF	01/04/16	02/07/17	451	14.83	0	0
C24	D	01/04/16	09/01/18	638	20.97	1	0
C25	D	01/04/16	12/01/18	641	21.07	1	Liver, Lung
C31	R	01/04/16	12/03/18	701	23.04	1	0
C41	R	01/04/16	13/05/18	762	25.05	1	Liver, WAT, Ovary
V27	VEGF	01/04/16	07/10/18	906	29.78	1	WAT
C43	R	03/04/16	14/06/18	791	26.00	1	Liver
C50	D	03/04/16	15/10/18	912	29.98	1	Lung, Liver
V34	VEGF	03/04/16	27/10/18	924	30.37	1	Spleen
V42	VEGF	03/04/16	18/01/19	1005	33.04	1	0
V44	VEGF	03/04/16	24/02/19	1041	34.22	1	0
C28	D	05/04/16	09/02/18	664	21.83	1	Kidney
C44	D	05/04/16	17/06/18	792	26.04	1	0
C49	R	05/04/16	22/09/18	887	29.16	1	0
V28	VEGF	05/04/16	08/10/18	903	29.68	1	0
V30	VEGF	05/04/16	18/10/18	913	30.01	1	Ovary, Liver
V45	VEGF	05/04/16	26/02/19	1041	34.22	1	0
C32	R	06/04/16	17/03/18	701	23.04	1	0
C45	R	06/04/16	18/06/18	792	26.04	1	Spleen, Ovary, Liver
V25	VEGF	06/04/16	23/09/18	887	29.16	1	0
V29	VEGF	06/04/16	08/10/18	902	29.65	1	0
V40	VEGF	06/04/16	30/12/18	984	32.35	1	0
V46	VEGF	06/04/16	27/02/19	1041	34.22	1	WAT
V13	VEGF	10/05/16	13/09/17	483	15.88	0	0
C46	D	10/05/16	19/06/18	759	24.95	1	Spleen, Skin
C47	VEGF	10/05/16	25/07/18	795	26.13	1	Spleen
C48	R	10/05/16	11/08/18	811	26.66	1	Liver

V37	VEGF	10/05/16	12/11/18	902	29.65	1	0
V21	VEGF	14/05/16	28/03/18	674	22.16	0	0
V22	VEGF	14/05/16	28/03/18	674	22.16	0	0
C35	D	14/05/16	10/04/18	686	22.55	1	Spleen, Liver
C36	D	14/05/16	25/04/18	701	23.04	1	WAT, Liver
C39	R	14/05/16	30/04/18	706	23.21	1	Spleen, Liver
C40	D	14/05/16	06/05/18	712	23.41	1	Liver
V36	VEGF	14/05/16	08/11/18	894	29.39	1	Liver
V23	VEGF	17/05/16	01/04/18	674	22.16	0	0
C37	D	17/05/16	27/04/18	700	23.01	1	Liver
V38	VEGF	17/05/16	19/11/18	902	29.65	1	0

Table S2.

Genotype, lifespan and presence of tumors at the time of death for all male mice used in survival studies.
Horizontal red lines separate different litters.
Genotype: D- mice harboring only the driver transgene; R- mice harboring only the VEGF responder transgene; VEGF- double transgenic mice harboring both driver and responder transgenes.
Lifespan: Mice were euthanized when clinical signs suggested death within 24 hours or, in some cases, died naturally.
Censored mice (0): Reasons for censoring the indicated mice were–C34, C35, C36, V29 and V41 suffered from ear/skin dermatitis resistant to antibiotics treatment. C29 and V23, V21 and V22, V7 and V8 presented severe fight injuries. V1, V2, V3, V4, V5 presented prolapsed penis due to cysts in the reproductive glands. V25 and V33 presented rectal prolapse. C26, C28, C33, V6, V15, V24 and V35 presented foot injury and self- mutilation.

Otherwise, these mice did not present any clinical sign suggesting imminent death. Tumors: presence of apparent neoplastic lesions at the time of sacrifice and the affected organs.

Tumors: presence of apparent neoplastic lesions at the time of sacrifice and the affected organs

Mouse ID	Gene	Date of birth	Date of death	Age at death (Days)	Age at death (Months)	Censored (0) Included (1)	Neoplastic lesion in indicated organ
C4	R	05/12/14	03/08/16	598	19.66	1	Spleen, WAT, Liver
V2	VEGF	05/12/14	18/08/16	613	20.15	0	0
V11	VEGF	05/12/14	04/05/17	869	28.57	1	0
V12	VEGF	05/12/14	10/05/17	875	28.76	1	0
C2	R	17/12/14	06/07/16	559	18.38	1	0
C3	D	17/12/14	16/07/16	569	18.70	1	Skin
C11	D	17/12/14	19/11/16	692	22.75	1	Liver, Kidney
V16	VEGF	17/12/14	25/10/17	1028	33.79	1	0
V26	VEGF	17/12/14	15/01/18	1108	36.42	1	0
C5	D	01/01/15	29/08/16	598	19.66	1	Spleen, WAT
V7	VEGF	01/01/15	21/11/16	680	22.35	0	0
V8	VEGF	01/01/15	21/11/16	680	22.35	0	0
C6	R	12/01/15	14/09/16	602	19.79	1	0
V4	VEGF	12/01/15	10/11/16	658	21.63	0	0
C14	R	12/01/15	17/02/17	755	24.82	1	Spleen, Skin, Epididymis
V20	VEGF	12/01/15	25/12/17	1063	34.94	1	0
V1	VEGF	15/01/15	25/06/16	520	17.09	0	0
C7	D	15/01/15	28/09/16	613	20.15	1	0
C17	R	15/01/15	20/04/17	815	26.79	1	Spleen, Liver, Lung
C19	D	15/01/15	27/07/17	912	29.98	1	Spleen, WAT, Liver

V17	VEGF	15/01/15	30/10/17	1005	33.04	1	0
V28	VEGF	15/01/15	17/02/18	1112	36.55	1	0
V3	VEGF	01/02/15	25/08/16	564	18.54	0	0
C10	D	01/02/15	17/11/16	646	21.24	1	Spleen
V10	VEGF	01/02/15	20/03/17	769	25.28	1	Spleen, Liver, SG
V27	VEGF	01/02/15	18/01/18	1067	35.08	1	WAT
C1	D	02/02/15	30/03/16	418	13.74	1	0
C8	D	02/02/15	02/10/16	600	19.72	1	0
V18	VEGF	02/02/15	08/12/17	1026	33.73	1	0
V30	VEGF	02/02/15	22/02/18	1100	36.16	1	Spleen
V5	VEGF	28/02/15	11/11/16	613	20.15	0	0
C12	D	28/02/15	26/12/16	658	21.63	1	Skin, Spleen, WAT
V31	VEGF	28/02/15	28/02/18	1080	35.50	1	0
V32	VEGF	28/02/15	06/03/18	1088	35.77	1	0
C9	D	01/03/15	12/10/16	581	19.10	1	0
V6	VEGF	01/03/15	14/11/16	613	20.15	0	0
C13	D	01/03/15	28/12/16	657	21.60	1	Liver, Spleen
V34	VEGF	01/03/15	25/04/18	1134	37.28	1	0
V9	VEGF	09/03/15	15/01/17	666	21.89	1	WAT, SG
C15	D	09/03/15	19/02/17	700	23.01	1	WAT, Liver, Spleen, Epididymis
C16	D	09/03/15	01/03/17	712	23.41	1	WAT, Liver, Lung, Epididymis
V13	VEGF	09/03/15	15/07/17	846	27.81	1	0
V14	VEGF	09/03/15	01/08/17	862	28.34	1	WAT
C20	R	08/03/16	19/08/17	521	17.13	1	0
C24	R	08/03/16	08/11/17	600	19.72	1	0
V36	VEGF	08/03/16	28/04/18	770	25.31	1	0
C26	R	10/03/16	11/12/17	631	20.74	0	0
V24	VEGF	10/03/16	08/01/18	658	21.63	0	0
C38	R	10/03/16	20/03/18	730	24.00	1	Liver, Spleen, WAT, Epididymis
V38	VEGF	10/03/16	15/06/18	815	26.79	1	WAT, colon
V49	VEGF	10/03/16	14/05/19	1144	37.61	1	0
V15	VEGF	15/03/16	08/10/17	563	18.51	0	0
C21	R	15/03/16	09/10/17	564	18.54	1	0
C22	D	15/03/16	20/10/17	575	18.90	1	0
C23	D	15/03/16	20/10/17	575	18.90	1	Liver, Lung, WAT
V35	VEGF	15/03/16	27/04/18	762	25.05	0	WAT, Spleen
C31	D	18/03/16	04/02/18	676	22.22	1	0
C44	R	18/03/16	18/05/18	780	25.64	1	Liver, Lung, Spleen, Epididymis
V37	VEGF	18/03/16	23/05/18	785	25.81	1	WAT, Kidney
V42	VEGF	18/03/16	22/09/18	904	29.72	1	0

C30	R	20/03/16	12/01/18	652	21.43	1	0
V25	VEGF	20/03/16	12/01/18	652	21.43	0	0
V33	VEGF	01/04/16	11/04/18	730	24.00	0	0
C41	D	01/04/16	26/04/18	745	24.49	1	Liver, Spleen, SG
C43	D	01/04/16	14/05/18	763	25.08	1	0
V40	VEGF	01/04/16	24/07/18	833	27.38	1	0
C49	R	01/04/16	01/10/18	900	29.59	1	Liver, WAT, Spleen, Lung, Epididymis
V48	VEGF	01/04/16	28/04/19	1107	36.39	1	0
C27	R	03/04/16	16/12/17	613	20.15	1	0
C28	D	03/04/16	01/01/18	628	20.64	0	0
C32	D	03/04/16	05/02/18	662	21.76	1	0
V43	VEGF	03/04/16	06/10/18	903	29.68	1	0
C18	R	05/04/16	24/05/17	409	13.45	1	0
V21	VEGF	05/04/16	03/01/18	628	20.64	0	0
V22	VEGF	05/04/16	06/01/18	631	20.74	0	0
C47	D	05/04/16	21/06/18	796	26.17	1	Liver
C48	R	05/04/16	19/07/18	824	27.09	1	WAT, Spleen, Liver, SG
V47	VEGF	05/04/16	18/04/19	1093	35.93	1	0
C29	D	06/04/16	07/01/18	631	20.74	0	0
V23	VEGF	06/04/16	07/01/18	631	20.74	0	0
C39	D	06/04/16	08/04/18	722	23.73	1	Liver, WAT
C40	D	06/04/16	15/04/18	729	23.96	1	Liver, Spleen
V45	VEGF	06/04/16	18/01/19	1002	32.94	1	0
C25	D	10/05/16	26/11/17	556	18.28	1	0
C45	R	10/05/16	01/06/18	741	24.36	1	0
C46	R	10/05/16	05/06/18	745	24.49	1	WAT, Liver, Spleen, Epididymis
C50	D	10/05/16	07/01/19	957	31.46	1	WAT, Spleen, Liver, Lung
V50	VEGF	10/05/16	25/05/19	1095	36.00	1	WAT, Spleen
C33	R	14/05/16	14/02/18	630	20.71	0	0
C37	R	14/05/16	11/03/18	657	21.60	1	0
V39	VEGF	14/05/16	04/07/18	770	25.31	1	WAT
V46	VEGF	14/05/16	02/04/19	1038	34.12	1	0
V19	VEGF	17/05/16	18/12/17	571	18.77	1	0
C34	D	17/05/16	18/02/18	631	20.74	0	0
C42	R	17/05/16	30/04/18	703	23.11	1	Spleen, Liver
V44	VEGF	17/05/16	30/11/18	913	30.01	1	0
C35	D	20/05/16	21/02/18	631	20.74	0	0
C36	D	20/05/16	21/02/18	631	20.74	0	0

| V29 | VEGF | 20/05/16 | 21/02/18 | 631 | 20.74 | 0 | 0 |
| V41 | VEGF | 20/05/16 | 03/09/18 | 823 | 27.05 | 0 | 0 |

Table S3.

Levels of plasma VEGF (pg/ml) measured in all female mice used for lifespan studies.

VEGF levels in censored mice are indicated in bold.

Months	2	4	6	8	10	12	14	16	18	20	22	24	26	28	30	32	34	36
V1	**90**	**87**	**94**	**101**														
C1	56	79	67	89	89	61	110											
C2	83	95	93	101	74	63	112	119										
V4	**95**	**79**	**95**	**96**	**108**	**182**	**167**	**187**	**174**	**150**								
V16	98	71	108	110	101	102	119	182	188	176	189	193	176	208	209	219		
C4	70	100	107	76	98	99	92	89	107									
C10	87	57	94	135	85	82	101	119	181	99	99							
C13	96	55	99	78	122	68	92	72	82	128	152	128						
V7	83	94	86	123	129	156	119	142	178	190	198	203	210	173				
V15	82	90	94	136	176	193	172	156	176	194	183	195	198	224	217			
C3	77	76	102	99	73	87	94	121										
C7	99	87	107	81	67	78	93	93	114									
C8	56	123	59	98	68	89	83	72	92	197								
V6	**86**	**92**	**91**	**90**	**122**	**173**	**182**	**192**	**172**	**197**	**187**	**192**						
V17	81	70	107	84	178	199	192	159	192	203	192	186	201	198	201			
V3	**93**	**82**	**89**	**124**	**162**	**157**	**154**	**164**										
C5	90	99	110	85	91	93	89	92	118									
C6	112	92	85	93	73	81	89	78	125									
V9	85	76	114	97	186	164	152	123	162	192	186	143	201					
V18	84	84	90	113	114	116	183	192	176	147	209		209		200	254		
V2	96	78	101	112	154	139	186											
C9	101	98	85	76	93	102	78	75	82	101								
V8	91	78	90	131	167	182	162	176	198	193	175	189	190					
V11	76	75	122	83	132	148	135	172	195	154	186	165	172	189				
V12	88	85	90	131	135	176	148	197	203	190	198	197	165	217				
V14	84	89	84	121	128	193	162	195	202	178	184	182	194	218	190			
C12	86	92	99	78	110													
C18	61	59	110	107	58	87	85	82	119									
C23	110	99	96	65	95	93	85	66	91	99								
C42	73	111	83	69	114	114	121	152	129	173	142	151	156					
V19	**90**	**91**	**89**	**113**	**135**	**153**	**182**	**192**	**192**	**167**								
V31	69	87	101	79	112	152	153	164	172	201	198	210	208	204	232			
V50	87	79	116	110	122	149	112	165	185	195	198	201	189	213	205	221	217	209
C11	80	87	90	89	111													
C22	104	93	75	99	83	87	99	88	90	127								
C26	68	101	86	72	88	99	98	81	93	93	120							
V33	74	88	99	125	114	122	120	172	156	189	187	201	198	178	239			
V47	87	92	124	125	138	162	162	177	189	198	199	210		221		217	203	
V49	90	85	99	132	127	119	154	157	191	190	201	216		234		214	229	217
C14	74	76	108	82	93	108												
C16	87	89	73	102	78	91	112											
C21	104	98	83	96	71	90	67	92	84	177								
C27	94	117	102	94	105	84	59	83	101	82	118							
V20	**73**	**49**	**89**	**110**	**98**	**93**	**87**	**92**	**82**	**102**	**123**							
V35	78	92	91	96	182	186	128	164	178	195	179	198	201	231	271			

V41	79	83	98	124	93	126	146	167	174	193	199	203		208		210	
C15	104	98	86	75	82	115											
C19	48	84	93	101	82	82	98	85	128								
C29	95	55	72	108	103	98	83	99	102	110	134						
C33	68	68	101	62	103	83	90	88	109	132	145	171					
V24	86	79	93	127	125	129	126	165	192	179	178	164	183	175			
V32	93	85	92	145	190	143	201	124	182	198	199	187	193	159	176		
V39	78	82	110	99	102	121	162	190	192	182	198	210	195	224	196		
V5	**76**	**92**	**94**	**98**	**102**	**148**											
C17	73	96	89	85	81	97	102										
C20	66	110	74	89	63	93	78	85	127								
C30	65	62	71	65	107	94	94	117	128	142	119						
C34	64	53	110	98	141	99	78	81	88	127	161	125					
C38	89	71	91	86	126	104	78	72	89	98	89	178					
V26	92	94	118	112	125	156	182	121	173	191	193	197	204	190	210		
V43	91	78	94	134	126	110	187	183	182	195	178	198		204		212	249
V48	88	96	121	126	146	148	151	182	168	212	208	198		210		178	196
V10	**86**	**85**	**105**	**105**	**167**	**171**	**157**										
C24	98	90	84	98	84	90	76	99	71	83							
C25	62	102	86	69	63	104	87	99	128	110							
C31	59	86	81	89	112	89	110	99	108	129	121						
C41	88	69	98	94	102	114	85	91	100	126	110	143					
V27	76	79	108	90	172	187	132	178	189	204	175	203	189	169			
C43	64	89	82	79	101	108	108	119	106	145	179	138					
C50	88	53	78	84	121	109	112	109	104	126	119	172	178	193	231		
V34	95	86	99	108	117	176	199	132	165	173	201	200	97	199	198		
V42	86	96	99	118	99	182	142	194	190	187	190	201	211	198	219	189	
V44	89	79	92	142	129	128	193	164	178	199	203	193		203		199	213
C28	59	102	108	64	99	93	78	102	118	108							
C44	106	92	82	75	90	108	112	120	123	145	110	117	143				
C49	81	98	81	65	117	107	120	143	108	125	156	182	172	245			
V28	87	65	99	99	162	176	121	182	193	193	192	191	191	191			
V30	89	92	86	131	124	176	152	192	210	185	194	174	184	199	202		
V45	84	69	99	127	131	103	165	152	187	201	207	201		201		201	253
C32	100	84	79	97	151	77	89	97	119	129	128						
C45	72	80	96	78	112	120	123	127	119	132	138	129	156				
V25	72	95	69	111	142	192	152	158	201	202	153	167	183	210			
V29	75	83	83	89	133	134	139	123	176	210	128	185	208	198			
V40	88	94	106	106	110	114	126	177	190	188	146	199	209	178	200	223	
V46	86	90	118	139	142	151	173	169	198	201	204	189		195		200	216
V13	**67**	**88**	**94**	**90**	**116**	**142**	**192**										
C46	71	49	90	76	138	98	91	101	135	106	119	156					
C47	83	90	95	91	93	100	110	102	189	167	210	167	148				
C48	68	107	84	77	125	101	117	174	123	144	129	142	167				
V37	89	90	87	98	126	148	178	198	210	225	165	214	205	217			
V21	**94**	**117**	**102**	**94**	**105**	**84**	**59**	**83**	**101**	**82**	**118**						
V22	**67**	**83**	**93**	**89**	**112**	**86**	**99**	**89**	**92**	**72**	**156**						
C35	67	83	93	89	112	86	99	89	92	72	156						
C36	87	67	72	89	87	108	88	90	98	102	89						
C39	71	76	106	86	117	99	101	97	125	106	95						
C40	93	66	102	57	99	107	89	99	99	121	132						

V36	78	99	91	109	164	156	155	143	199	187	203	210	186	205			
V23	**89**	**69**	**98**	**88**	**147**	**137**	**182**	**199**	**210**	**189**	**186**						
V38	84	99	93	122	154	156	110	201	208	197	189	218	194	199			
C37	95	55	72	108	103	98	83	99	102	110	134						

Table S4.

Levels of plasma VEGF (pg/ml) measured in all male mice used for lifespan studies.

VEGF levels in censored mice are indicated in bold

Months	2	4	6	8	10	12	14	16	18	20	22	24	26	28	30	32	34	36
C4	70	78	82	106	98	98	92	89	107									
V2	**73**	**61**	**80**	**97**	**137**	**124**	**208**	**178**	**223**	**198**								
V11	77	97	69	97	165	141	181	111	167	181	197	202	210	187				
V12	69	78	72	93	159	161	119	130	159	163	205	185	203	196				
C2	56	79	67	89	89	61	90	87	92									
C3	73	96	89	85	81	97	87	87	107									
C11	59	76	81	89	112	89	88	99	108	129	121							
V16	55	65	89	84	85	106	171	178	186	172	202	189	201	221	197	199		
V26	70	82	73	82	102	125	123	170	157	146	168	169	136	187	175	196	192	196
C5	62	92	85	93	73	69	89	78	125									
V7	**59**	**62**	**93**	**82**	**125**	**149**	**176**	**109**	**190**	**135**	**207**							
V8	77	60	65	108	112	141	191	120	149	216	170							
C6	61	59	62	107	58	76	85	82	119									
V4	**66**	**52**	**77**	**73**	**112**	**122**	**191**	**170**	**204**	**179**								
C14	88	69	98	106	102	114	121	132	100	126	110	143						
V20	61	67	69		97	88	192	180	170	137	213	202	215		201	249	229	
V1	**67**	**70**	**73**	**86**	**118**	**105**	**125**	**181**										
C7	66	89	74	87	63	65	78	85	127	123								
C17	72	80	84	78	112	120	123	127	119	132	138	129	156					
C19	81	88	81	65	117	107	120	143	108	125	134	182	172	245	210			
V17	59	73	73	121	108	178	191	144	172	184	187	174	204	221	218	203		
V28	64	75	103	119	121	95	171	165	183	188	203	202		218		212	184	196
V3	**63**	**68**	**84**	**90**	**150**	**156**	**166**	**187**										
C10	68	86	78	90	88	99	98	81	93	93								
V10	78	49	48	96	125	177	184	160	192	192	157	159						
V27	63	79	78	124	82	136	151	182	166	177	194	193	217	195	220	184	260	
C1	68	92	99	78	110	118												
C8	48	94	83	101	82	98	98	85	128									
V18	58	53	86	69	100	184	201	147	186	193	196	166	207	195	202	211		
V30	63	73	97	103	125	167	182	157	192	191	208	181		192		195	207	209
V5	**44**	**71**	**73**	**75**	**99**	**127**	**191**	**203**	**212**	**208**								
C12	73	49	89	110	98	93	87	92	82	102								
V31	56	66	77	111	76	133	155	155	150	183	203	195		205		205	195	
V32	68	61	73	110	109	147	196	171	172	185	182	190		201		207	216	
C9	90	99	83	85	91	96	89	92	118									
V6	**70**	**65**	**68**	**109**	**130**	**142**	**171**	**152**	**178**	**198**								
C13	67	83	93	89	112	86	99	89	92	72								
V34	67	68	78	127	110	113	163	145	185	180	205	208		231		209	223	222
V9	61	68	69	116	118	167	163	180	180	181	196							
C15	56	74	79	97	151	77	89	97	119	129	128							
C16	71	76	86	86	117	99	93	97	125	106	95							
V13	62	87	53	75	173	172	162	186	183	194	179	190	195					
V14	72	63	61	106	95	178	129	180	196	168	188	187	200	215				

C20	47	76	98	82	93	108	89	112										
C24	99	87	87	81	67	99	93	93	114									
V36	82	55	70	94	147	141	207	131	171	177		207	202					
C26	**56**	**59**	**82**	**82**	**68**	**89**	**83**	**72**	**92**	**197**								
V24	**60**	**84**	**65**	**95**	**145**	**141**	**195**	**166**	**195**	**180**								
C38	56	55	99	118	122	68	92	72	156	128	124	128						
V38	73	66	66	83	109	133	195	162	204	215	169	206	211					
V49	64	62	95	112	105	134	121	153	179	185	202	193	195	210	206	216	220	210
V15	**53**	**75**	**73**	**83**	**85**	**133**	**156**	**171**										
C21	87	89	73	102	78	91	92	99	102									
C22	83	95	93	101	74	63	88	119	108									
C23	77	76	102	99	73	89	94	121	116									
V35	**58**	**53**	**101**	**68**	**115**	**133**	**173**	**152**	**189**	**144**	**178**	**186**						
C31	65	62	71	65	107	94	94	117	128	142	119							
C44	73	83	99	93	99	124	128	123	105	142	123	126						
V37	66	62	52	74	116	119	214	180	170	200	132	177						
V42	46	80	70	64	155	137	141	160	184	191	202	188	214	201				
C30	54	117	73	94	105	84	59	83	101	82								
V25	**55**	**70**	**62**	**117**	**169**	**134**	**144**	**189**	**131**	**173**								
V33	**62**	**63**	**72**	**112**	**108**	**114**	**181**	**112**	**191**	**169**	**189**	**192**						
C41	71	49	90	96	138	112	91	101	123	106	119	156						
C43	64	79	82	79	101	108	108	119	106	145	179	138						
V40	48	78	64	84	145	161	210	187	187	183	196	183	197					
C49	73	85	83	69	114	114	121	152	129	173	122	151	156	167	154			
V48	65	79	100	109	129	111	160	170	162	202	212	190		207		173	206	189
C27	54	98	83	113	71	64	67	92	84	177								
C28	**98**	**84**	**90**	**99**	**84**	**72**	**76**	**99**	**71**	**83**								
C32	75	55	72	108	103	98	83	99	102	110								
V43	70	71	68	130	161	128	130	153	176	188	203	191	199	206				
C18	67	87	90	89	111	123												
V21	**85**	**90**	**101**	**87**	**94**	**111**	**126**	**164**	**140**	**128**								
V22	**72**	**62**	**74**	**81**	**170**	**167**	**161**	**196**	**168**	**140**								
C47	68	52	82	75	90	108	112	120	123	145	110	117	143					
C48	68	77	84	77	125	101	117	144	123	144	129	142	167					
V47	66	62	71	117	112	104	202	152	170	189	207	185		200		194	218	
C29	**84**	**75**	**93**	**78**	**83**	**87**	**99**	**88**	**90**	**127**								
V23	**67**	**74**	**68**	**98**	**105**	**138**	**128**	**188**	**186**	**157**								
C39	63	66	82	57	99	107	89	99	99	121	132							
C40	68	68	71	62	103	83	90	88	118	132	145							
V45	55	75	70	81	107	171	161	152	176	185	183	195	207	228	272	254		
C25	54	98	86	75	82	115	89	98	132									
C45	64	53	69	108	141	115	78	81	99	127	161	125						
C46	89	71	91	99	126	104	112	123	134	98	82	178						
C50	88	53	78	84	121	109	112	109	104	126	119	172	178	193	208			
V50	61	52	78	95	114	101	174	140	181	191	211	193		198		196	205	246
C33	**62**	**86**	**79**	**81**	**63**	**104**	**87**	**99**	**128**	**110**								
C37	87	57	94	135	85	82	78	119	181	99								
V39	68	65	69	116	118	161	202	185	214	180	202	189						
V46	65	77	85	91	93	99	135	165	184	178	150	179	215	175	201	218	225	
V19	70	67	87	100	124	137	128	154	157									
C34	**56**	**85**	**98**	**87**	**93**	**102**	**78**	**75**	**82**	**101**								

C42	87	67	72	89	87	108	88	90	98	102		89				
V44	51	78	71	110	111	107	171	146	168	179		191	193	204	175	240
C35	78	96	99	93	95	93	85	66	91	99						
C36	59	98	81	90	99	93	78	102	118	108						
V29	64	66	66	92	150	132	135	166	140	124						
V41	82	72	61	107	137	141	208	124	202	187		193	210	200		

References and Notes

1. S. Rafii, J. M. Butler, B. S. Ding, Angiocrine functions of organ-specific endothelial cells. *Nature* **529**, 316–325 (2016). doi:10.1038/nature17040 Medline

2. Z. Ungvari, S. Tarantini, T. Kiss, J. D. Wren, C. B. Giles, C. T. Griffin, W. L. Murfee, P. Pacher, A. Csiszar, Endothelial dysfunction and angiogenesis impairment in the ageing vasculature. *Nat. Rev. Cardiol.* **15**, 555–565 (2018). doi:10.1038/s41569-018-0030-z Medline

3. D. G. Le Couteur, E. G. Lakatta, A vascular theory of aging. *J. Gerontol. A Biol. Sci. Med. Sci.* **65**, 1025–1027 (2010). doi:10.1093/gerona/glq135 Medline

4. B. J. North, D. A. Sinclair, The intersection between aging and cardiovascular disease. *Circ. Res.* **110**, 1097–1108 (2012). doi:10.1161/CIRCRESAHA.111.246876 Medline

5. M. S. Goligorsky, Microvascular rarefaction: The decline and fall of blood vessels. *Organogenesis* **6**, 1–10 (2010). doi:10.4161/org.6.1.10427 Medline

6. A. P. Kusumbe, S. K. Ramasamy, R. H. Adams, Coupling of angiogenesis and osteogenesis by a specific vessel subtype in bone. *Nature* **507**, 323–328 (2014). doi:10.1038/nature13145 Medline

7. Y. Hasegawa, T. Saito, T. Ogihara, Y. Ishigaki, T. Yamada, J. Imai, K. Uno, J. Gao, K. Kaneko, T. Shimosawa, T. Asano, T. Fujita, Y. Oka, H. Katagiri, Blockade of the nuclear factor-κB pathway in the endothelium prevents insulin resistance and prolongs life spans. *Circulation* **125**, 1122–1133 (2012). doi:10.1161/CIRCULATIONAHA.111.054346 Medline

8. A. Das, G. X. Huang, M. S. Bonkowski, A. Longchamp, C. Li, M. B. Schultz, L. J. Kim, B. Osborne, S. Joshi, Y. Lu, J. H. Treviño-Villarreal, M. J. Kang, T. T. Hung, B. Lee, E. O. Williams, M. Igarashi, J. R. Mitchell, L. E. Wu, N. Turner, Z. Arany, L. Guarente, D. A. Sinclair, Impairment of an endothelial NAD^+-H_2S signaling network is a reversible cause of vascular aging. *Cell* **173**, 74–89.e20 (2018). doi:10.1016/j.cell.2018.02.008 Medline

9. S. Tarantini, M. N. Valcarcel-Ares, P. Toth, A. Yabluchanskiy, Z. Tucsek, T. Kiss, P. Hertelendy, M. Kinter, P. Ballabh, Z. Süle, E. Farkas, J. A. Baur, D. A. Sinclair, A. Csiszar, Z. Ungvari, Nicotinamide mononucleotide (NMN) supplementation rescues cerebromicrovascular endothelial function and neurovascular coupling responses and improves cognitive function in aged mice. *Redox Biol.* **24**, 101192 (2019). doi:10.1016/j.redox.2019.101192 Medline

10. M. B. Chen, A. C. Yang, H. Yousef, D. Lee, W. Chen, N. Schaum, B. Lehallier, S. R. Quake, T. Wyss-Coray, Brain endothelial cells are exquisite sensors of age-related circulatory cues. *Cell Rep.* **30**, 4418–4432.e4 (2020). doi:10.1016/j.celrep.2020.03.012 Medline

11. A. J. Barinda, K. Ikeda, D. B. Nugroho, D. A. Wardhana, N. Sasaki, S. Honda, R. Urata, S. Matoba, K. I. Hirata, N. Emoto, Endothelial progeria induces adipose tissue senescence

and impairs insulin sensitivity through senescence associated secretory phenotype. *Nat. Commun.* **11**, 481 (2020). [doi:10.1038/s41467-020-14387-w](#) [Medline](#)

12. A. Lazarus, E. Keshet, Vascular endothelial growth factor and vascular homeostasis. *Proc. Am. Thorac. Soc.* **8**, 508–511 (2011). [doi:10.1513/pats.201102-021MW](#) [Medline](#)

13. A. S. Maharaj, M. Saint-Geniez, A. E. Maldonado, P. A. D'Amore, Vascular endothelial growth factor localization in the adult. *Am. J. Pathol.* **168**, 639–648 (2006). [doi:10.2353/ajpath.2006.050834](#) [Medline](#)

14. D. May, D. Gilon, V. Djonov, A. Itin, A. Lazarus, O. Gordon, C. Rosenberger, E. Keshet, Transgenic system for conditional induction and rescue of chronic myocardial hibernation provides insights into genomic programs of hibernation. *Proc. Natl. Acad. Sci. U.S.A.* **105**, 282–287 (2008). [doi:10.1073/pnas.0707778105](#) [Medline](#)

15. T. Licht, G. Rothe, T. Kreisel, B. Wolf, O. Benny, A. G. Rooney, C. Ffrench-Constant, G. Enikolopov, E. Keshet, VEGF preconditioning leads to stem cell remodeling and attenuates age-related decay of adult hippocampal neurogenesis. *Proc. Natl. Acad. Sci. U.S.A.* **113**, E7828–E7836 (2016). [doi:10.1073/pnas.1609592113](#) [Medline](#)

16. K. Furrer, A. Rickenbacher, Y. Tian, W. Jochum, A. G. Bittermann, A. Käch, B. Humar, R. Graf, W. Moritz, P. A. Clavien, Serotonin reverts age-related capillarization and failure of regeneration in the liver through a VEGF-dependent pathway. *Proc. Natl. Acad. Sci. U.S.A.* **108**, 2945–2950 (2011). [doi:10.1073/pnas.1012531108](#) [Medline](#)

17. T. Takahashi, S. Yamaguchi, K. Chida, M. Shibuya, A single autophosphorylation site on KDR/Flk-1 is essential for VEGF-A-dependent activation of PLC-gamma and DNA synthesis in vascular endothelial cells. *EMBO J.* **20**, 2768–2778 (2001). [doi:10.1093/emboj/20.11.2768](#) [Medline](#)

18. R. L. Kendall, K. A. Thomas, Inhibition of vascular endothelial cell growth factor activity by an endogenously encoded soluble receptor. *Proc. Natl. Acad. Sci. U.S.A.* **90**, 10705–10709 (1993). [doi:10.1073/pnas.90.22.10705](#) [Medline](#)

19. C. E. Riera, A. Dillin, Tipping the metabolic scales towards increased longevity in mammals. *Nat. Cell Biol.* **17**, 196–203 (2015). [doi:10.1038/ncb3107](#) [Medline](#)

20. J. L. Kuk, T. J. Saunders, L. E. Davidson, R. Ross, Age-related changes in total and regional fat distribution. *Ageing Res. Rev.* **8**, 339–348 (2009). [doi:10.1016/j.arr.2009.06.001](#) [Medline](#)

21. I. H. Kim, T. Kisseleva, D. A. Brenner, Aging and liver disease. *Curr. Opin. Gastroenterol.* **31**, 184–191 (2015). [doi:10.1097/MOG.0000000000000176](#) [Medline](#)

22. M. Ogrodnik, S. Miwa, T. Tchkonia, D. Tiniakos, C. L. Wilson, A. Lahat, C. P. Day, A. Burt, A. Palmer, Q. M. Anstee, S. N. Grellscheid, J. H. J. Hoeijmakers, S. Barnhoorn, D. A. Mann, T. G. Bird, W. P. Vermeij, J. L. Kirkland, J. F. Passos, T. von Zglinicki, D.

Jurk, Cellular senescence drives age-dependent hepatic steatosis. *Nat. Commun.* **8**, 15691 (2017). doi:10.1038/ncomms15691 Medline

23. S. B. Ballak, H. Degens, A. de Haan, R. T. Jaspers, Aging related changes in determinants of muscle force generating capacity: A comparison of muscle aging in men and male rodents. *Ageing Res. Rev.* **14**, 43–55 (2014). [doi:10.1016/j.arr.2014.01.005](doi:10.1016/j.arr.2014.01.005) Medline

24. R. K. Sayed, E. C. de Leonardis, J. A. Guerrero-Martínez, I. Rahim, D. M. Mokhtar, A. M. Saleh, K. E. Abdalla, M. J. Pozo, G. Escames, L. C. López, D. Acuña-Castroviejo, Identification of morphological markers of sarcopenia at early stage of aging in skeletal muscle of mice. *Exp. Gerontol.* **83**, 22–30 (2016). doi:10.1016/j.exger.2016.07.007 Medline

25. E. V. Menshikova, V. B. Ritov, L. Fairfull, R. E. Ferrell, D. E. Kelley, B. H. Goodpaster, Effects of exercise on mitochondrial content and function in aging human skeletal muscle. *J. Gerontol. A Biol. Sci. Med. Sci.* **61**, 534–540 (2006). doi:10.1093/gerona/61.6.534 Medline

26. S. Salvioli, M. Capri, S. Valensin, P. Tieri, D. Monti, E. Ottaviani, C. Franceschi, Inflamm-aging, cytokines and aging: State of the art, new hypotheses on the role of mitochondria and new perspectives from systems biology. *Curr. Pharm. Des.* **12**, 3161–3171 (2006). [doi:10.2174/138161206777947470](doi:10.2174/138161206777947470) Medline

27. M. J. Yousefzadeh, M. J. Schafer, N. Noren Hooten, E. J. Atkinson, M. K. Evans, D. J. Baker, E. K. Quarles, P. D. Robbins, W. C. Ladiges, N. K. LeBrasseur, L. J. Niedernhofer, Circulating levels of monocyte chemoattractant protein-1 as a potential measure of biological age in mice and frailty in humans. *Aging Cell* **17**, e12706 (2018). doi:10.1111/acel.12706 Medline

28. G. C. Leonardi, G. Accardi, R. Monastero, F. Nicoletti, M. Libra, Ageing: From inflammation to cancer. *Immun. Ageing* **15**, 1 (2018). [doi:10.1186/s12979-017-0112-5](doi:10.1186/s12979-017-0112-5) Medline

29. B. G. Hughes, S. Hekimi, Different mechanisms of longevity in long-lived mouse and *Caenorhabditis elegans* mutants revealed by statistical analysis of mortality rates. *Genetics* **204**, 905–920 (2016). doi:10.1534/genetics.116.192369 Medline

30. D. May, V. Djonov, G. Zamir, M. Bala, R. Safadi, M. Sklair-Levy, E. Keshet, A transgenic model for conditional induction and rescue of portal hypertension reveals a role of VEGF-mediated regulation of sinusoidal fenestrations. *PLOS ONE* **6**, e21478 (2011). doi:10.1371/journal.pone.0021478 Medline

31. G. Zhao, X. W. Cheng, L. Piao, L. Hu, Y. Lei, G. Yang, A. Inoue, S. Ogasawara, H. Wu, C. N. Hao, K. Okumura, M. Kuzuya, The soluble VEGF receptor sFlt-1 contributes to impaired neovascularization in aged mice. *Aging Dis.* **8**, 287–300 (2017). [doi:10.14336/AD.2016.0920](doi:10.14336/AD.2016.0920) Medline

32. K. Wang, D. Wu, H. Zhang, A. Das, M. Basu, J. Malin, K. Cao, S. Hannenhalli, Comprehensive map of age-associated splicing changes across human tissues and their

contributions to age-associated diseases. *Sci. Rep.* **8**, 10929 (2018). doi:10.1038/s41598-018-29086-2 Medline

33. S. Rey, G. L. Semenza, Hypoxia-inducible factor-1-dependent mechanisms of vascularization and vascular remodelling. *Cardiovasc. Res.* **86**, 236–242 (2010). doi:10.1093/cvr/cvq045 Medline

34. R. Del Bo, S. Ghezzi, M. Scarlato, D. Albani, D. Galimberti, U. Lucca, M. Tettamanti, E. Scarpini, G. Forloni, N. Bresolin, G. P. Comi, Role of VEGF gene variability in longevity: A lesson from the Italian population. *Neurobiol. Aging* **29**, 1917–1922 (2008). doi:10.1016/j.neurobiolaging.2007.05.003 Medline

35. E. Zurita, M. Chagoyen, M. Cantero, R. Alonso, A. González-Neira, A. López-Jiménez, J. A. López-Moreno, C. P. Landel, J. Benítez, F. Pazos, L. Montoliu, Genetic polymorphisms among C57BL/6 mouse inbred strains. *Transgenic Res.* **20**, 481–489 (2011). doi:10.1007/s11248-010-9403-8 Medline

36. A. Kistner, M. Gossen, F. Zimmermann, J. Jerecic, C. Ullmer, H. Lübbert, H. Bujard, Doxycycline-mediated quantitative and tissue-specific control of gene expression in transgenic mice. *Proc. Natl. Acad. Sci. U.S.A.* **93**, 10933–10938 (1996). doi:10.1073/pnas.93.20.10933 Medline

37. Y. Dor, V. Djonov, R. Abramovitch, A. Itin, G. I. Fishman, P. Carmeliet, G. Goelman, E. Keshet, Conditional switching of VEGF provides new insights into adult neovascularization and pro-angiogenic therapy. *EMBO J.* **21**, 1939–1947 (2002). doi:10.1093/emboj/21.8.1939 Medline

38. J. F. Sun, T. Phung, I. Shiojima, T. Felske, J. N. Upalakalin, D. Feng, T. Kornaga, T. Dor, A. M. Dvorak, K. Walsh, L. E. Benjamin, Microvascular patterning is controlled by fine-tuning the Akt signal. *Proc. Natl. Acad. Sci. U.S.A.* **102**, 128–133 (2005). doi:10.1073/pnas.0403198102 Medline

39. A. Anisimov, A. Alitalo, P. Korpisalo, J. Soronen, S. Kaijalainen, V. M. Leppänen, M. Jeltsch, S. Ylä-Herttuala, K. Alitalo, Activated forms of VEGF-C and VEGF-D provide improved vascular function in skeletal muscle. *Circ. Res.* **104**, 1302–1312 (2009). doi:10.1161/CIRCRESAHA.109.197830 Medline

40. I. Knani, B. J. Earley, S. Udi, A. Nemirovski, R. Hadar, A. Gammal, R. Cinar, H. J. Hirsch, Y. Pollak, I. Gross, T. Eldar-Geva, D. P. Reyes-Capo, J. C. Han, A. M. Haqq, V. Gross-Tsur, R. Wevrick, J. Tam, Targeting the endocannabinoid/CB1 receptor system for treating obesity in Prader-Willi syndrome. *Mol. Metab.* **5**, 1187–1199 (2016). doi:10.1016/j.molmet.2016.10.004 Medline

41. D. C. Simonson, R. A. DeFronzo, Indirect calorimetry: Methodological and interpretative problems. *Am. J. Physiol.* **258**, E399–E412 (1990). Medline

42. K. W. Cho, D. L. Morris, C. N. Lumeng, Flow cytometry analyses of adipose tissue macrophages. *Methods Enzymol.* **537**, 297–314 (2014). doi:10.1016/B978-0-12-411619-1.00016-1 Medline

43. N. Laws, A. Hoey, Progression of kyphosis in mdx mice. *J. Appl. Physiol.* **97**, 1970–1977 (2004). doi:10.1152/japplphysiol.01357.2003 Medline